NASA
Technical
Paper
2609

September 1986

Directivity and Trends of Noise Generated by a Propeller in a Wake

P. J. W. Block and
Garl L. Gentry, Jr.

NASA

NASA
Technical
Paper
2609

1986

Directivity and Trends of Noise Generated by a Propeller in a Wake

P. J. W. Block and
Garl L. Gentry, Jr.

Langley Research Center
Hampton, Virginia

National Aeronautics
and Space Administration

**Scientific and Technical
Information Branch**

Contents

Summary

An experimental study of the effects on far-field propeller noise of pylon wake interaction was conducted with a scale model of a single-rotation propeller in a low-speed anechoic wind tunnel. A detailed mapping of the noise directivity was obtained at 10 test conditions covering a wide range of propeller power loadings at several subsonic tip speeds. Two types of noise penalties were investigated–"pusher" and "spacing." The pusher noise penalty is the difference in the average overall sound pressure level, OASPL, for pusher and tractor installations. (In a pusher installation, the propeller disk is downstream of a pylon or another aerodynamic surface.) The spacing noise penalty is the difference in the average OASPL for different distances between the pylon trailing edge and the propeller. The variations of these noise penalties with axial, or flyover, angle θ and circumferential angle ϕ are presented, and the trends in these noise penalties with tip Mach number and power loading are given for selected values of θ and ϕ.

The circumferential directivity of the noise from a pusher installation showed that the additional noise due to the interaction of the pylon wake with the propeller had a broad peak over a wide range of circumferential angles approximately perpendicular to the pylon with a sharp minimum 90° to the pylon for the majority of cases tested. The variation of the pusher noise penalty with θ had a minimum occurring near the propeller plane and maximum values of as much as 20 dB occurring toward the propeller axes. The magnitude of the pusher noise penalty generally decreased as propeller tip Mach number or power loading was increased; however, the penalty did not decrease to zero in all directions.

The noise data measured for pylon spacings of 0.1c and 0.3c (c is the pylon chord) were analyzed similarly. The directivity comparisons showed that both a noise reduction and a change in the directivity pattern resulted when the pylon was moved further from the propeller.

Introduction

Design proposals for the next generation of subsonic aircraft show a shift from turbofans to advanced high-speed propellers or unducted-fan propulsion systems. The new propeller designs for these propulsion systems promise large savings in fuel economy resulting in lower direct operating costs. One technical concern for these propulsion concepts, however, is their noise levels, since the propellers operate without a duct that absorbs sound around them. References 1 and 2 show that current technology in propeller noise prediction yields confident estimates of the noise from single-rotation (SR) propellers in a uniform inflow. Reference 1 contains a description of two time-domain acoustic formulations and their implementation on a computer. These formulations, which were developed by Farassat, were shown to give good agreement with wind-tunnel noise data for the SR-1 and SR-3 propeller designs. The same formulations were compared with noise data from an SR-2 propeller operating at zero and nonzero pitch and in a counterrotation configuration in reference 2. Again, good agreement was found between the measurements and the predictions. The comparison for the counterrotation configuration was limited to the first harmonic, where the dominant source was the sum of the noise from the individual propellers and not from the wake interaction. The experimental results contained in references 3 and 4, however, show the importance of the wake interaction on the propeller noise field. The technology needed to predict and control the additional noise caused by the wakes going into the propeller disk is not yet available and requires experimental data for study and validation.

The source of this additional noise has been the subject of several experimental studies, and a bibliography of those studies which focuses on aircraft installations is presented in reference 3. These studies show that the amount of noise increase depends on the observer (microphone) location and the propeller operating conditions. However, none of the experiments address in a systematic way the question of how operating conditions such as tip Mach number or power loading influence the directivity and magnitude of the noise penalty. This information can be used by aircraft designers to minimize these penalties. Also lacking in the literature are noise data on the effects of pylon spacing and type of attachment to the engine nacelle.

This paper focuses on the additional noise (or noise penalty) associated with a single-rotation propeller operating in a wake. Presented are the results of a scale model experimental study which addresses the effects of operating conditions on the magnitude as well as the directivity of pusher propeller noise. The operational parameters chosen for evaluation were the helical tip Mach number ($0.456 \leq M_T \leq 0.722$), and the power loading normalized by the propeller diameter squared and the number of propeller blades ($0.12 \leq (\mathrm{SHP}/d^2)/B \leq 4.26$). The study was conducted in a low-speed anechoic wind tunnel at a free-stream speed of 120 fps. The far-field radiated noise was mapped over a range covering 110° to the propeller axis (flyover angle) and up to 340° circumferentially. The data are presented as overall sound pressure level (OASPL) versus circumferential

angle in polar plots. The variation of the difference in OASPL between the tractor and pusher installations (noise penalty) is plotted against the axial angle and the circumferential angle. The effect of pylon-to-propeller spacing is similarly presented. The trends in the noise penalties with tip Mach number and power loading are presented and indicate the penalties beyond the range tested. These trends are given for selected axial and circumferential angles. Finally, the directivity for two different pylon attachments is presented.

Symbols

Dimensional quantities are presented in both U.S. Customary Units and the International System of Units (SI). Measurements and calculations were made in U.S. Customary Units.

a_n, b_n, c_n	Fourier coefficients
B	number of blades in propeller
c	pylon chord, in.
c_a	ambient sound speed
C_P	power coefficient, $P/\rho n^3 d^5$
C_T	thrust coefficient, $T/\rho n^2 d^4$
d	propeller diameter, in. or ft
e_1, e_2, e_3	polynomial coefficients
J	propeller advance ratio, U/nd
M_T	helical tip Mach number, $\sqrt{U^2 + (\pi nd)^2}/c_a$
n	shaft rotation speed, revolutions per second
P	power absorbed by propeller
$(\mathrm{SHP}/d^2)/B$	power loading per blade, $\mathrm{hp/ft^2}$
T	propeller thrust
U	tunnel free-stream velocity, fps
β	angle of propeller section chord with respect to plane of rotation, deg
$\beta_{.75}$	geometric pitch of propeller airfoil section at 75 percent of its radius, deg
Δ	noise penalty calculated as difference in noise between two propeller installations (see eq. (1)), dB
θ	polar angle of microphone measurement with respect to propeller axis (see fig. 7), deg
ρ	air density
ϕ	circumferential angle of microphone measurement with respect to pylon (see fig. 7), deg

Abbreviations:

AVG	average
LHR	left-hand rotation
OASPL	overall sound pressure level, dB re 20 μPa
PCA	pitch change axis
QFF	Quiet Flow Facility
RHR	right-hand rotation
RMS	root-mean-square difference between polynomial curve fit of equation (2) and calculated value of average difference (e.g., see fig. 17)
SHP	shaft horsepower
SR	single rotation

Description of Experimental Setup

Hardware and Facility

An overall view of the experimental setup for the far-field measurements is shown in figure 1. The figure shows the single-rotation pusher installation mounted vertically over the open jet in the Quiet Flow Facility (QFF) in the Langley Aircraft Noise Reduction Laboratory. The vertically traversing microphone measurement array was arranged on a circular arc around the propeller. Dimensional and nondimensional information is found in table I.

Propeller and hub. A modified SR-2 propeller design was used for this study. The SR-2 is an unswept high-speed advanced propeller design with an activity factor of 203. The diameter was 16.1 in. (0.409 m). A drawing of the modified SR-2 propeller computational model is given in figure 2. The twist and chord distributions are given in figure 3(a), and a representative set of airfoil sections are given in figure 3(b). The blades were fabricated from aluminum on a numerically controlled milling machine and were dynamically balanced after assembly with the spinner and hub. The hub permitted a continuous range of blade angle settings. Two, four, or eight

blades could be mounted in the hub. For this test, both four- and eight-blade configurations were used. The collective blade angle was set to an accuracy of $\pm 0.25°$ by means of a blade-mold fixture which was fitted to one blade. The blade angle given in this paper is the average angle of the set of blades at the 75-percent radial station. An opposite-rotation SR-2 propeller was also used to examine the effect of rotational direction on the directivity characteristics of the noise for a single-rotation pusher propeller. Normal operation of the propeller was right-handed, that is, clockwise looking upstream. For the four-blade pusher propeller test series, both left-hand rotation and right-hand rotation were used.

Nacelles and pylons. The nacelles were straight cylinders tapered at the nose with a maximum outside diameter of 6 in. (0.15 m). The nacelle downstream of the propeller housed a 29-hp water-cooled electric motor (10 000 rpm). A dummy nacelle was used upstream of the propeller in conjunction with the pylons to simulate the pusher configuration as shown in figure 1.

The pylons had symmetric airfoil sections with a constant chord, c, of 15 in. (0.381 m). The airfoil section coordinates are shown in figure 4. Two different nacelle-to-pylon attachments were designed to produce a radial pylon and a tangent, or offset, pylon as shown in figure 5. For the radial pylon, the chord plane was aligned along a radius of the nacelle, and for the tangent pylon, the chord plane was tangent to the outside surface of the nacelle. The radial pylon was adjustable in the streamwise, or flight, direction. The two positions used in this test placed the trailing edge of the pylon $0.1c$ (1.5 in., 0.0381 m) and $0.3c$ (4.5 in., 0.114 m) upstream of the pitch change axis (PCA) of the propeller. The tangent pylon was not adjustable, and the trailing-edge-to-PCA distance was $0.2c$ (3 in., 0.076 m).

Microphone array. The far-field microphone array was located on a circular arc boom outside of the flow. (See fig. 1.) Eleven ½-inch-diameter microphones fitted with wind screens of open cell foam were arranged every 20° on the arc. A plan view of the microphone boom is shown in figure 6. The angle ϕ described the circumferential position of the microphones relative to the pylon. The first microphone was located at 10°, and the last, at 210°. The boom was traversed vertically to obtain axial (or flyover) measurements at 12 positions corresponding to increments of 10° beginning at $\theta = 30°$ relative to the direction of flight (propeller axis) and ending at $\theta = 140°$. (See fig. 7.) The spatial distribution of all the measurement points is shown in figure 7. The large dots represent the 132 measurement positions.

Quiet Flow Facility (QFF). The QFF, located at the NASA Langley Research Center (LaRC), is a large anechoic room with a very low turbulence quiet flow supply. A complete description of the flow and anechoic characteristics of the QFF is given in reference 5. In the present investigation, the low-pressure air system provided the forward velocity through a 4-ft (1.22-m) diameter vertical jet. The pitch change axis of the propeller was 58 in. (1.48 m) above the exit of the jet. The test matrix was designed to allow sufficient potential core between the propeller tips and the shear layer so that no correction to the propeller force data was required. The position and flow characteristics of the potential core and shear layer of the jet with an operating propeller are documented in reference 6.

Test Conditions

Hardware configurations. Table II describes the conditions under which data were obtained for this test. The number of propeller blades and the blade pitch setting at the 75-percent radial station are listed in the first two columns of table II. Rotational speeds of 7200, 9500, and 11 400 rpm were tested and corresponded to rotational tip speeds of 506, 667, and 801 fps (154, 203, and 244 m/s), respectively. The nominal free-stream velocity for all tests was 120 fps (36.6 m/s). The propellers were tested in both a tractor installation and a pusher installation. In the pusher installation, a pylon was placed upstream of the propeller disk and was attached to a dummy nacelle as described previously. Both left-hand rotation (LHR) and right-hand rotation (RHR) were employed for the pusher installations.

Operating conditions. Table III lists the operating conditions and parameters which were calculated from the measured thrust and torque of the propeller. These parameters include the thrust coefficient, C_T, the power coefficient, C_P, and the power loading, $(\mathrm{SHP}/d^2)/B$.

Data Reduction and Method of Presentation

The microphone data were high-pass filtered at 80 Hz and recorded on 1-in. magnetic tape at 60 ips. A once-per-revolution pulse, which was generated by an optic sensor on the shaft, was also recorded for data analysis purposes. The recorded data were digitized using the once-per-revolution pulse to obtain 512 points of data for each revolution of the shaft.

A minimum of 120 revolutions of data was stored for each microphone (61 440 points). Fourier analysis was used on each revolution of data to produce the sine and cosine coefficients for the first 25 harmonics of the blade passage frequency (a_n and b_n, respectively; $n = 1, 2, \ldots, 25$). These coefficients were averaged over the 120 revolutions of data to yield $\bar{a}_n$ and $\bar{b}_n$. The amplitude of the noise contribution for each of the harmonics was computed from the averaged Fourier coefficients by using

$$c_n = \left(\bar{a}_n^2 + \bar{b}_n^2\right)^{1/2}$$

and converted to decibels. These harmonic levels were computed for each of the 132 microphone locations. The OASPL for each microphone location was then computed as the sum of the mean square amplitudes of each of the harmonics. Only the OASPL data are presented and analyzed in this paper. The levels of the first four harmonics, which contained most of the sound intensity, generally followed the same directivity pattern and the same trends as the OASPL for the range of measurement angles and operating conditions reported herein. Spectral analysis of the data also showed no significant contribution beyond the fifteenth harmonic. No shear layer corrections have been applied to the data, nor have the data been normalized to a constant radius.

The directivity of the data is presented in terms of the angles θ and ϕ. The axial angle θ was measured from the upstream propeller axis, or the flight direction. (See fig. 7.) The angle ϕ describes the circumferential position and was measured from the radial pylon; ϕ was positive in the counterclockwise direction looking upstream. Polar plots of the data are presented for six axial angles θ to display the directivity and compare the relative noise levels of a pusher installation and a tractor installation. An example is given in figure 8, which shows the pylon position at $\phi = 0°$, the direction of propeller right-hand rotation, RHR, and a typical set of RHR and LHR data. The open symbols in figure 8 present the data measured for the RHR propeller, and the solid symbols, the LHR. For the radial pylon configurations, the LHR data provided, via symmetry, the directivity for $150° \leq \phi \leq 350°$. Symmetry is assumed here, since the pylon was symmetric and was at an angle of attack of 0° with respect to the uniform airstream. For configurations for which both LHR and RHR data were obtained, they are coplotted to give the directivity from 10° to 350°. Since the measurement arc extended beyond $\phi = 180°$, there were four data points which overlapped, namely $\phi = 150°$, 170°, 190°, and 210°. Otherwise, the measurement array shown in figure 7 provides data for $10° \leq \phi \leq 210°$ only. The level of the noise from the tractor configuration is shown by a dashed line and corresponds to the average over ϕ of the square of the pressure of the measured tractor levels. The value Δ is the noise penalty at the given axial angle, θ. Since the noise from a pusher installation varied circumferentially (that is, with ϕ), it is helpful to characterize the noise increase at a given axial angle by a single value which is an average over the circumferential angles. This value, Δ, was obtained by averaging the pressure squared values for the pusher installation over ϕ to obtain the average pusher level at the given angle θ and then subtracting the average tractor level in accordance with the relation

$$\Delta = \mathrm{OASPL}_{\mathrm{AVG,pusher}} - \mathrm{OASPL}_{\mathrm{AVG,tractor}} \quad (1)$$

where

$$\mathrm{OASPL}_{\mathrm{AVG}} = 10 \log_{10}\left(\frac{1}{N}\sum_{j=1}^{N} 10^{\mathrm{OASPL}_j/10}\right) \quad (2)$$

Here OASPL denotes the measured noise level in decibels, and N corresponds to the number of measurements in the average. In the example of figure 8, the pusher data varied from 7 dB below the average tractor level ($\phi = 350°$) to about 7 dB above it ($270° \leq \phi \leq 310°$). The noise penalty associated with the pusher installation in this case was 3.4 dB at $\theta = 91°$. Producing an average from several measurements will aide in describing the overall trends and directional characteristics of the wake interaction noise associated with a pusher installation. In a similar manner, an average over the axial angles was calculated for a given circumferential angle using equation (1). For this average, the value of N was 12 for the 12 axial measurement positions ($\theta = 30°$, 40°, ..., 140°). The same procedure for assessing the noise penalty was applied to other configuration changes such as the pylon spacing change.

Equation (1) is one of several ways in which a noise penalty may be calculated. An alternative method involves subtracting the tractor level in decibels from the pusher level in decibels and then averaging the differences. This procedure would yield slightly lower penalties than equations (1) and (2), since equation (2) tends to emphasize the larger numbers in the average. The data were analyzed both ways. The maximum difference between the two described methods was 2.6 dB.

The quantity Δ, which is a measure of the average change in noise associated with the wake (and

will also be referred to as the noise penalty), was also examined as a function of propeller operating conditions such as absorbed horsepower and helical tip Mach number. The trends of Δ with $(\mathrm{SHP}/d^2)/B$ and M_T were characterized by second-order least squares polynomial curves at selected values of θ and ϕ. The polynomial coefficients, e_i, for each curve are given in the figures and were defined from the polynomial expression

$$\Delta(x) = e_1 + e_2 x + e_3 x^2 \qquad (3)$$

In this expression, x represents either M_T or $(\mathrm{SHP}/d^2)/B$. Thus a relationship between $(\mathrm{SHP}/d^2)/B$ or M_T and the noise penalty produced by the propeller in a wake was assumed.

When the effect of the spacing between the pylon trailing edge and the propeller PCA is discussed, the noise penalty is defined as the difference between the average measured noise level at spacings of $0.3c$ and $0.1c$ (c is the pylon chord) and is associated with placing the pylon trailing edge closer to the propeller disk.

Radial Pylon Results

Noise Comparisons of Pusher and Tractor Installations

Directivity. Polar plots of the directivity of the noise (OASPL) from a pusher installation (propeller plus pylon) are given in figures 9 through 12. These plots compare the noise levels for the pusher propeller at the closer pylon spacing with those of the tractor (no pylon). Figures 9 and 10 present the four-blade propeller results for $\beta_{.75} = 18.8°$ and $24.0°$, respectively, and figures 11 and 12 show the eight-blade propeller data at $\beta_{.75} = 20.0°$ and $30.0°$. A set of six polar plots are given at each rotational speed tested (cf. table II). The penalty Δ is given by equations (1) and (2) for each value of θ. The data showed that the greatest noise increases occurred over a wide range of circumferential angles approximately perpendicular to the pylon. The noise data peaked for $30° < \phi < 140°$ and for $270° < \phi < 330°$ regardless of the axial angle θ or the number of blades. For the higher rotational speeds (9500 and 11 400 rpm), a sharp decrease in the noise was observed normal to the pylon ($\phi = 90°$). This dip, which became apparent slightly ahead of the propeller plane ($\theta = 70°$), remained in the directivity pattern downstream of the propeller ($\theta = 130°$). The dip was more pronounced for the four-blade propeller (figs. 9(b), 9(c), 10(b), and 10(c)), although it was also apparent for the eight-blade propeller (fig. 11(c)). In this direction ($\phi = 90°$), the pusher was actually as quiet as or quieter than the tractor for the higher propeller speeds aft of the propeller plane. Decreases in noise of more than 10 dB were measured in the plane of the propeller (figs. 9(c) and 11(c)). Examination of the pressure time history of the data (not shown) on either side of the dip ($\phi = 70°$ and $110°$) revealed that the noise signal had undergone a phase change of 180°. The left-hand rotation data showed that the dip in the directivity occurred only on the side of the pylon away from the advancing propeller blade. The presence of the dip is not attributed to shielding because it occurred near and behind the propeller plane and not in front of it, where the pylon was located. It is conjectured that this dip resulted from the cancellation of the sound fields from two sources of similar magnitude, namely, the steadily and unsteadily loaded propeller blades.

The directivity patterns in figures 9 through 12 also showed that the least effect on the noise from the pylon wake occurred parallel to the pylon ($\phi = 180°$). In this general direction, particularly for the higher rotational speeds, the pusher levels equaled those of the tractor. The exceptions to this general behavior occurred at the upstream angles ($\theta \leq 50°$).

Finally, of note in all the data in figures 9 through 12 is that the peak noise levels associated with the pusher propeller were approximately constant irrespective of the flyover angle, θ. On the other hand, the tractor data exhibited minimum values toward the axes and a maximum near the propeller plane of rotation. For this reason, the largest increase in noise, Δ, occurred upstream of the propeller (at $\theta = 30°$).

Variation of pusher noise penalty with θ and ϕ. The noise penalty Δ, or difference in the average OASPL between the pusher and tractor installations, as a function of θ and ϕ is given in figures 13 through 16. Figures 13 and 14 present the results for the four-blade propeller with $\beta_{.75} = 18.8°$ and $24.0°$, respectively. Figures 15 and 16 show the eight-blade configurations with $\beta_{.75} = 20.0°$ and $30.0°$. The data indicated that the pusher installation penalties consistently decreased with increasing rotational speed. Since the blade angle was fixed, a reduction in the rotational speed resulted in a lower power loading as well. The variations in the penalty as a function of θ were simple U-shaped curves with the minimum noise penalty occurring near the plane of rotation and maximum values toward the axes ($\theta = 30°$ and $140°$). In some cases, as much as a 20-dB noise penalty was added to the tractor noise for $\theta = 30°$. Applied to an actual flyover, this result indicates that an aircraft with a pusher-installed propeller would be detected

before a tractor installation, and it would also be heard for a longer period of time.

The noise penalty variations with ϕ were typically M-shaped with minimum values occurring parallel to the pylon ($\phi = 10°$ and 180°). The direction $\phi = 10°$ corresponds approximately to the fuselage location. An additional minimum occurred at $\phi = 90°$ for the higher rotational speeds. These trends were observed for both four- and eight-blade propellers. Maximum noise penalties occurred for $\phi = 60°$ and 120° and for $270° < \phi < 310°$.

It may be noted that the calculated noise penalties for figures 13 and 14 were almost equal even though the power loading for the data of figure 14 is two to four times higher than that for the data of figure 13.

Trends in pusher noise penalty with $(\mathrm{SHP}/d^2)/B$ ***and*** M_T**.** This section of the paper presents the relationship between the magnitude of the noise penalty for a pusher installation and the operational parameters $(\mathrm{SHP}/d^2)/B$ and M_T. The noise penalty, Δ, is plotted against $(\mathrm{SHP}/d^2)/B$ and M_T in figures 17 and 18 for selected values of θ and in figures 19 and 20 for selected values of ϕ. The 10 test conditions (see table III) resulted in 10 values of $(\mathrm{SHP}/d^2)/B$ ranging from 0.12 to 4.26 hp/ft^2 and 3 values of M_T from 0.456 to 0.722. Noise penalties outside of this range are inferred from the data trends.

Given in the figures along with the data points are the least squares curve fit, the polynomial coefficients e_1, e_2, and e_3 for equation (3), and the root-mean-square difference (RMS) between the least squares curve and the data points. The data of figures 17 and 18 show that, in general, the noise penalty for the pusher installation decreased as the chosen operational parameters increased. Thus the interaction noise component was larger than the steady noise component for lower power loadings and lower tip Mach numbers regardless of the angle θ or ϕ. For higher loadings and tip Mach numbers, the penalty approached zero in the propeller plane of rotation ($\theta = 90°$). However, toward the upstream axis ($\theta \leq 50°$), the curves decreased to a noise penalty whose magnitude increased as θ decreased. That is, the axial contribution of the noise from the pusher installation did not decrease to zero with increasing power loading or tip Mach number. For $\theta = 30°$, the curves approached a level in excess of 15 dB, and for $\theta = 50°$, a level of about 10 dB was approached. Finally, of note in figures 17 and 18 is the fact that the noise penalty appeared to correlate better with M_T than with $(\mathrm{SHP}/d^2)/B$, as evidenced by the lower RMS values given on the right-hand side of each plot.

Figures 19 and 20 present the noise penalty trends at selected values of the circumferential angle, ϕ. In general, the pattern of the data followed that of the previous two figures. The main difference was the angles for which the curves failed to approach zero with increasing $(\mathrm{SHP}/d^2)/B$ and M_T. This behavior is observed in the data at $\phi = 50°$, where a penalty of about 5 dB was suggested by the data trends. Similarly, the curves for $\phi = 70°$, 110°, and 130° (not shown) did not approach zero. For $\phi = 90°$, the line representing the least squares curve fit approaches levels well below zero. This trend is a result of the sharp dip that occurred in the directivity pattern at $\phi = 90°$. The data in figure 20 showed another interesting feature, namely, that the four-blade data and the eight-blade data appeared to form separate lines. This behavior, which was more evident in the harmonics (not shown), indicates that the blade number or perhaps the blade passage frequency is another separate parameter on which the magnitude of the additional noise depends.

Effect of Pylon-to-Propeller Spacing

The focus of the data comparisons in the previous figures has been on the effect of a pylon wake on the propeller noise. For these comparisons, a pylon-to-propeller spacing of 0.1 pylon chord (c) was used. The effect of moving the pylon from a spacing of $0.3c$ to $0.1c$ was examined for all 10 test conditions. The directivity effects are presented in figures 21 through 24, the variation of the noise penalty with θ and ϕ is shown in figures 25 through 28, and the noise penalty trends with $(\mathrm{SHP}/d^2)/B$ and M_T are given in figures 29 through 32. For these presentations, the noise penalty was computed by subtracting the pusher propeller noise level measured with a spacing of $0.3c$ from that measured at $0.1c$ in accordance with equations (1) and (2). Thus the noise penalty associated with moving the trailing edge of the pylon closer to the propeller is termed the "spacing penalty."

Directivity. The directivity of the noise from the $0.3c$ pylon spacing is plotted along with that for the $0.1c$ spacing in figures 21 through 24. For the $0.3c$ spacing, no LHR data were obtained. The data comparisons for all 10 test conditions showed a general noise reduction when the pylon trailing edge was placed further from the propeller ($0.3c$). In addition to a change in the noise levels, a change in the shape was also evident. Of note is the change in the directivity pattern for the lowest rotational speed (7200 rpm). Figures 21(a) and 22(a) for the four-blade propeller show the dip at $\phi = 90°$ for the $0.3c$ spacing which was not present at the lower rotational

speeds for the closer 0.1c spacing. If the dip in the directivity pattern was produced by a cancellation of sound fields of similar magnitude, it is conceivable that increasing the pylon spacing would reduce the magnitude of the unsteady part to a level comparable to the steady part.

The data at the higher rotational speeds for the 0.3c spacing showed that the pusher noise levels were almost indistinguishable from those of the tractor near the plane of rotation ($70° < \theta < 130°$). Thus increasing the pylon trailing-edge-to-propeller spacing reduces the noise in this region. The 0.3c pylon spacing, however, showed a noticeable penalty toward the propeller axis.

Variation of spacing noise penalty with θ and ϕ. The average difference between the noise measured at 0.1c spacing and 0.3c spacing as a function of θ and ϕ is given in figures 25 through 28. The data trends were similar in some respects to those of figures 13 to 16. For the four-blade configurations shown in figures 25 and 26, the variation of Δ with θ was relatively flat with a maximum spacing penalty of about 10 dB, which occurs for $\theta = 30°$. As rotational speed increased, the spacing penalty increased for $\theta \leq 50°$ and decreased for $\theta > 50°$. The increase was more noticeable for the more lightly loaded propeller ($\beta_{.75} = 18.8°$). The variation of Δ with ϕ showed an M-shape with a maximum penalty of about 9 dB occurring at $\phi = 50°$ and $\phi = 130°$. The value of Δ at $\phi = 90°$ is related to the occurrence of the minimum in the directivity pattern. Because of the similarity of these results to those of figures 13 and 14, it is conceivable that a noticeable spacing penalty would also exist in the region $210° < \phi < 330°$.

The eight-blade data presented in figures 27 and 28 generally showed a higher spacing penalty than the four-blade data and approached a value of 15-dB. As in the four-blade results, the variation of Δ with θ was relatively flat for 7200 rpm and increased with increasing rotational speed for $\theta \leq 50°$ and decreased with increasing rotational speed for $\theta > 50°$.

Trends in spacing noise penalty with $(\mathrm{SHP}/d^2)/B$ and M_T. The effect of the operational parameters $(\mathrm{SHP}/d^2)/B$ and M_T on the difference in noise between the two pylon spacings is shown in figures 29 through 32 for selected values of θ and ϕ. In figures 29 and 30, the data showed that the noise penalty associated with a more closely spaced pylon increased with increasing $(\mathrm{SHP}/d^2)/B$ or M_T for $\theta = 30°$ and approached values over 10 dB. This reverse trend was unexpected and suggests that the noise penalty associated with a close spacing between the trailing edge of the pylon and the propeller disk will increase in the axial direction as the tip speed and/or power loading is increased. At $\theta = 50°$, the noise penalty remained relatively constant at about 8 to 10 dB as these parameters increased. For $\theta \geq 90°$, the data showed a decrease toward zero in the penalty associated with the close pylon spacing.

Figures 31 and 32 show the trends in the noise penalty at selected circumferential angles, ϕ. The data showed that the "spacing penalty" decreased with increasing $(\mathrm{SHP}/d^2)/B$ or M_T and approached zero for all values of ϕ.

Tangent Pylon Results

A tangential pylon attachment was designed to examine the effect on the noise of changing the wake pattern on the propeller disk. With the RHR tangent pylon, the propeller blade enters the wake more gradually than with the radial pylon, and the wake interaction begins at the inboard sections. (See fig. 5.) Thus it is expected that the interaction components of the noise change accordingly. Unfortunately, a hardware limitation placed the trailing edge of the pylon 0.2c from the PCA instead of 0.1c or 0.3c as with the radial pylon. For this reason, only limited tangent pylon data are presented with the radial pylon data at a spacing of 0.1c to show the change in the directivity characteristics.

Figure 33 presents the directivity for a tangent pylon (0.2c) and a radial pylon (0.1c) for the four-blade propeller at $\beta_{.75} = 24.0°$. Whereas the radial pylon data displayed a sharp dip 90° to the pylon, the tangent pylon data show decreases at $\phi = 50°$ and 130°. The resulting pattern is attributed to the change in the wake pattern on the unsteady part of the noise field. These directivity patterns were representative of the other tangent pylon cases.

Summary of Results

An experimental study of the effects of a pylon wake on far-field propeller noise was conducted with a scale model of a single-rotation propeller in a low-speed anechoic wind tunnel. A detailed mapping of the noise directivity was obtained at 10 test conditions covering tip Mach numbers, M_T of 0.456 to 0.722 and propeller power loadings, $(\mathrm{SHP}/d^2)/B$, of 0.12 to 4.26 hp/ft^2. The variation of the noise penalty between a tractor installation and a pusher installation (referred to as the "pusher penalty") with the flyover angle, θ, and the circumferential angle, ϕ, are presented. The noise penalties associated with a close versus a far pylon spacing (referred to as the "spacing penalty") are similarly presented. The trends in these noise penalties with M_T and $(\mathrm{SHP}/d^2)/B$ are given for selected values of θ and ϕ.

The circumferential directivity of the noise from a pusher installation showed that the additional noise due to the pylon wake peaked over a wide range of circumferential angles approximately perpendicular to the pylon. Under certain conditions of rotational speed and pylon spacing, a sharp decrease in the pusher noise was observed 90° to the pylon. In this direction, the pusher was as quiet as or quieter than the tractor installation.

The variations in the pusher noise penalty with θ were simple U-shaped curves with a minimum occurring in the propeller plane and maximum values of as much as 20 dB occurring toward the propeller axes. The pusher penalty variation with ϕ was characterized by M-shaped curves with minimum values occurring parallel to the pylon. An additional sharp minimum occurred at 90° to the pylon for the higher rotational speeds. Maximum noise penalties occurred for the circumferential angles $\phi = 60°$ and 120° and for $270° < \phi < 310°$.

The pusher installation noise penalties generally decreased as $(\mathrm{SHP}/d^2)/B$ or M_T increased. However, the penalties did not decrease to zero for all angles. In particular, the axial contribution of the noise from the pusher installation did not decrease to zero in all directions with increasing $(\mathrm{SHP}/d^2)/B$ or M_T but approached levels exceeding 10 dB for $\theta \leq 50°$.

Similarly, at circumferential angles of 50°, 70°, 110°, and 130° to the pylon, the pusher installation noise penalty did not approach zero with increasing $(\mathrm{SHP}/d^2)/B$ or M_T but approached a value of about 5 dB. These data also showed that the noise penalty correlated better with M_T than with $(\mathrm{SHP}/d^2)/B$. There is some evidence that the number of blades (or frequency) was an important factor in the noise increase.

Directivity comparisons between the noise measured for pylon spacings of $0.1c$ and $0.3c$ (c is the pylon chord) showed that both a noise reduction and some change in the directivity pattern were realized when the pylon trailing edge was moved further from the propeller. For the higher rotational speeds, the 0.3c spacing data were almost indistinguishable from the tractor installation data for $70° < \theta < 130°$. Analysis of the spacing penalty as a function of θ, ϕ, $(\mathrm{SHP}/d^2)/B$, and M_T showed that the penalty constantly increased with increasing $(\mathrm{SHP}/d^2)/B$ or M_T for $\theta = 30°$. That is, the closer pylon placement yielded higher axial noise penalties as M_T or $(\mathrm{SHP}/d^2)/B$ was increased. For $\theta \geq 90°$, the spacing penalty decreased with increasing M_T or $(\mathrm{SHP}/d^2)/B$.

The tangent pylon directivity showed a consistently different pattern than that observed with the radial pylon, with sharp decreases at $\phi = 50°$ and 130° instead of $\phi = 90°$.

NASA Langley Research Center
Hampton, VA 23665-5225
June 18, 1986

References

1. Nystrom, Paul A.; and Farassat, F.: *A Numerical Technique for Calculation of the Noise of High-Speed Propellers With Advanced Blade Geometry.* NASA TP-1662, 1980.
2. Block, Patricia J. W.: Acoustics of Advanced Turboprop Aircraft. *Langley Symposium on Aerodynamics, Volume II,* Sharon H. Stack, ed., NASA CP-2398, 1986, pp. 59–72.
3. Block, P. J. W.: *Experimental Study of the Effects of Installation on Single- and Counter-Rotation Propeller Noise.* NASA TP-2541, 1986.
4. Block, P. J. W.: Noise Radiation Patterns of Counter-Rotation and Unsteadily Loaded Single-Rotation Propellers. *J. Aircr.*, vol. 22, no. 9, Sept. 1985, pp. 776–783.
5. Hubbard, Harvey H.; and Manning, James C.: *Aeroacoustic Research Facilities at NASA Langley Research Center—Description and Operational Characteristics.* NASA TM-84585, 1983.
6. Block, P. J. W.: *Operational Evaluation of a Propeller Test Stand in the Quiet Flow Facility at Langley Research Center.* NASA TM-84523, 1982.

TABLE I. HARDWARE CHARACTERISTICS

	Dimensional	Nondimensional
Propeller:		
Diameter, d	16.10 in.	
Maximum chord	2.24 in.	0.139d
Hub diameter	4.50 in.	0.280d
Height above jet exit	58.0 in.	3.602d
Nacelles:		
Maximum diameter	6.0 in.	0.373d
Length, nose to PCA in pusher configuration	29.0 in.	1.80d
Pylons:		
Chord length, c	15.0 in.	0.932d
Maximum thickness	1.5 in.	0.1c
Trailing edge to PCA	1.5, 3.0, 4.5 in.	0.1c, 0.2c, 0.3c
Span of radial pylon for far-field study	23.813 in.	
Span of tangent pylon for far-field study	24.0 in.	
Microphone arrays:		
Diameter far-field microphones	1/2 in.	
Distance from propeller axis to far-field microphone	35.0 in.	2.174d
QFF:		
Length, width, height	20 × 30 × 25 ft	
Jet diameter	48 in.	2.98d

TABLE II. TEST CONDITIONS FOR WHICH FAR-FIELD DATA WERE OBTAINED

(a) Tractor configuration (no pylon)

No. of propeller blades, B	Pitch, $\beta_{.75}$, deg	Rotational speed, rpm
4	18.8	7200, 9500, and 11 400
4	24.0	7200, 9500, and 11 400
8	20.0	7200, 9500, and 11 400
8	30.0	7200

(b) Pusher configuration

No. of propeller blades, B	Pitch, $\beta_{.75}$, deg	Rotational speed, rpm	Propeller rotational direction	Pylon type	Spacing,[a] in.
4	18.8	7200, 9500, and 11 400	RHR	Radial	1.5 (0.1c) and 4.5 (0.3c)
			LHR	Radial	1.5 (0.1c)
			RHR	Tangent	3.0 (0.2c)
4	24.0	7200, 9500, and 11 400	RHR	Radial	1.5 (0.1c) and 4.5 (0.3c)
			LHR	Radial	1.5 (0.1c)
			RHR	Tangent	3.0 (0.2c)
			LHR	Tangent	3.0 (0.2c)
8	20.0	7200, 9500, 11 400	RHR	Radial	1.5 (0.1c) and 4.5 (0.3c)
			RHR	Tangent	3.0 (0.2c)
8	30.0	7200	RHR	Radial	1.5 (0.1c) and 4.5 (0.3c)
			RHR	Tangent	3.0 (0.2c)

[a]Distance between pylon trailing edge and PCA of propeller disk.

TABLE III. PROPELLER OPERATING CONDITIONS AND CALCULATED PARAMETERS

Propeller configuration		Calculated parameters for operating conditions of—								
		7200 rpm; $M_T = 0.456$; $J = 0.745$			9500 rpm; $M_T = 0.601$; $J = 0.564$			11 400 rpm; $M_T = 0.722$; $J = 0.470$		
Number of blades, B	Pitch, $\beta_{.75}$, deg	C_T	C_P	$(SHP/d^2)/B$, hp/ft^2	C_T	C_P	$(SHP/d^2)/B$, hp/ft^2	C_T	C_P	$(SHP/d^2)/B$, hp/ft^2
4	18.8	0.029	0.028	0.14	0.10	0.081	0.94	0.138	0.107	2.13
4	24.0	.111	.103	.52	.179	.175	2.0	.219	.214	4.26
8	20.0	.053	.048	.12	.154	.131	.73	.203	.168	1.61
8	30.0	.314	.400	1.0						

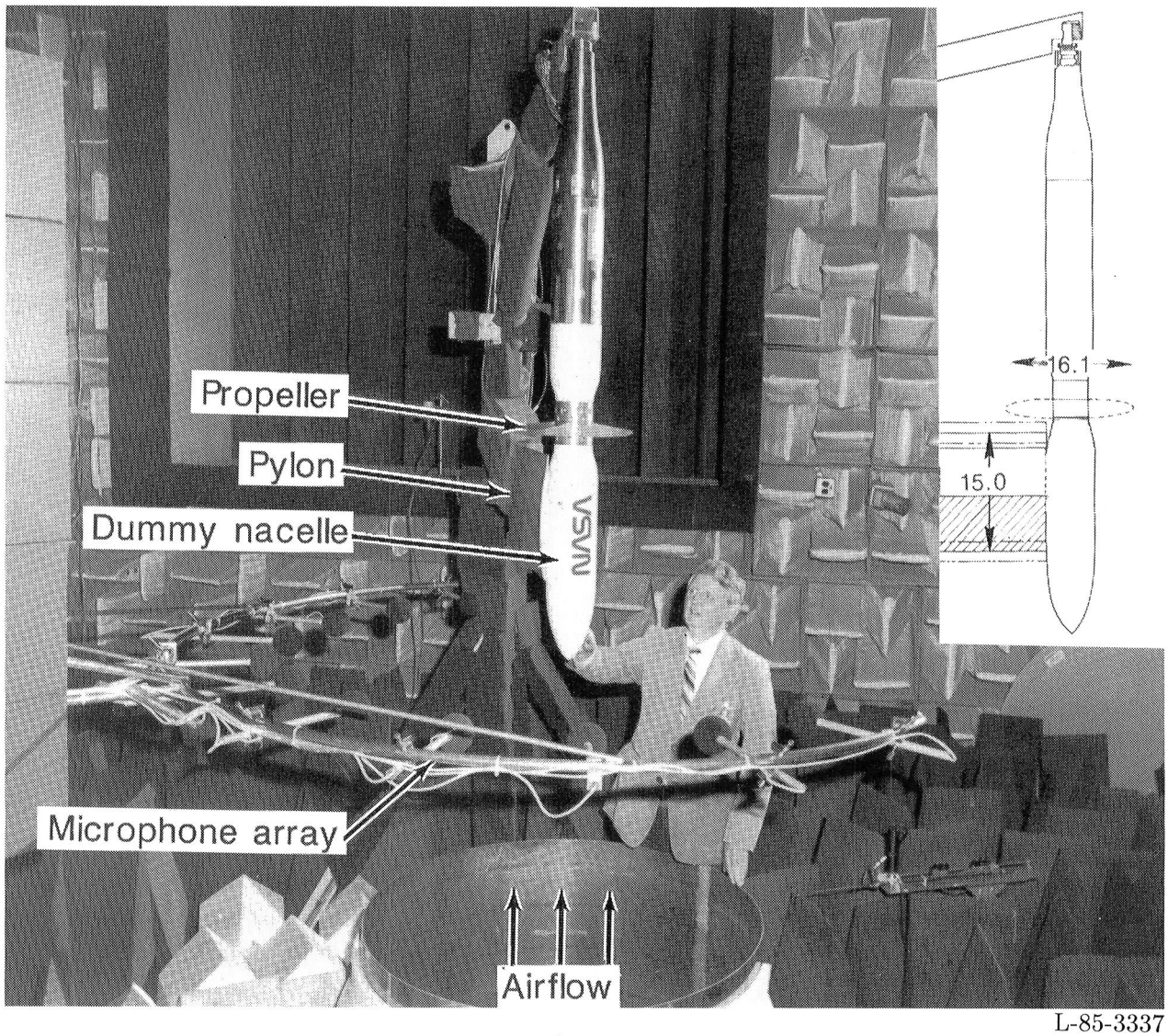

Figure 1. Test setup for pusher propeller noise study conducted in the QFF at NASA LaRC. Dimensions are in inches.

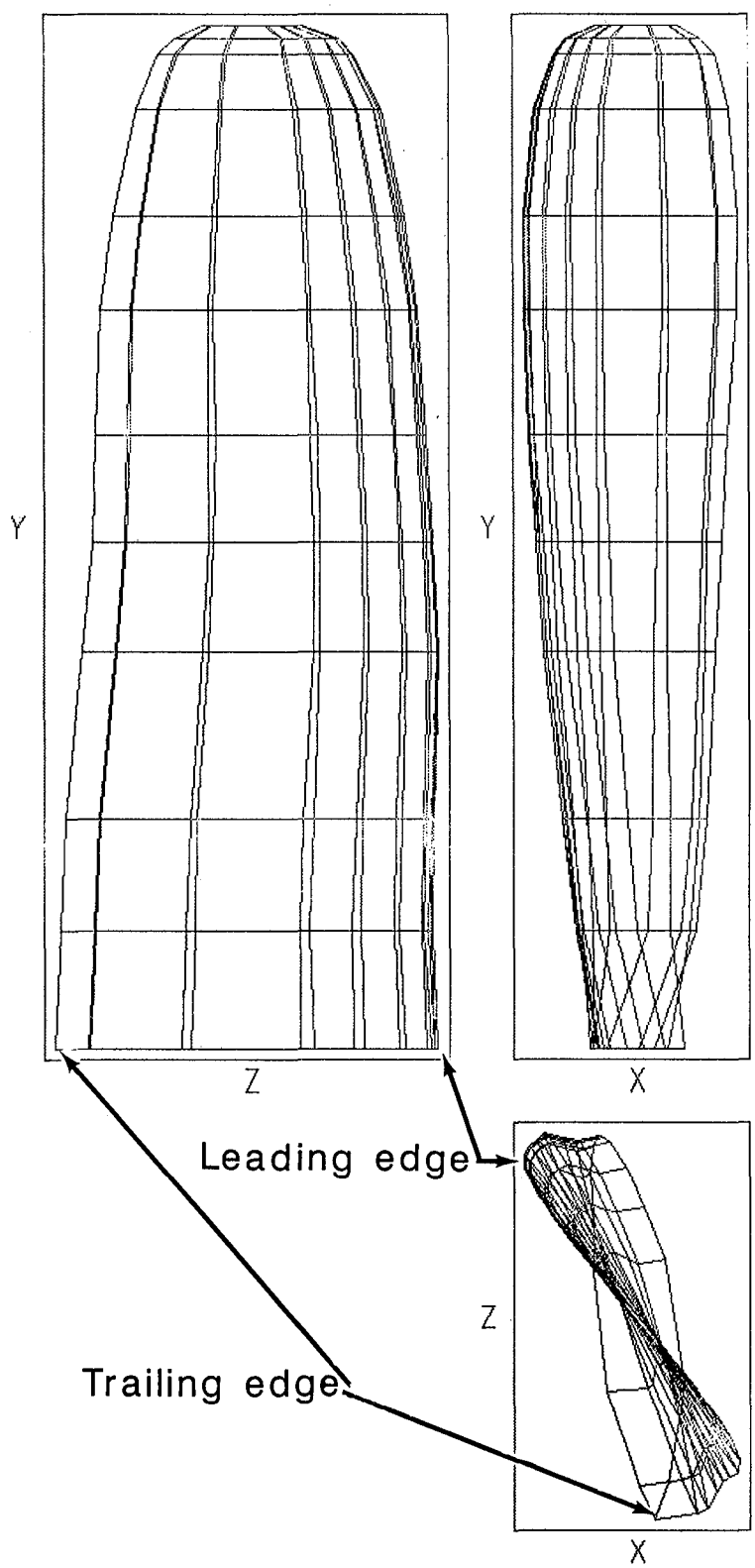

Figure 2. Three-dimensional drawing of modified SR-2 propeller used in this study.

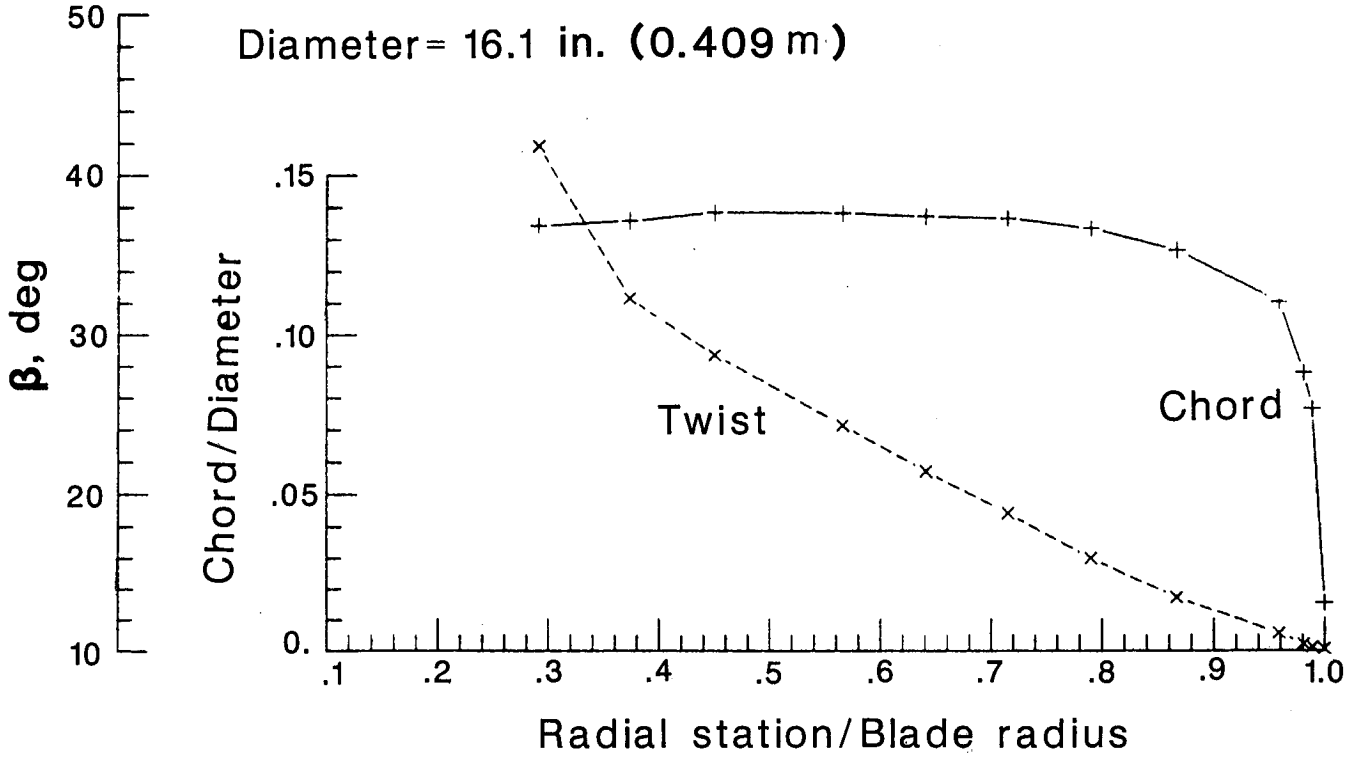

(a) Chord and twist distributions.

Figure 3. Description of modified SR-2 propeller.

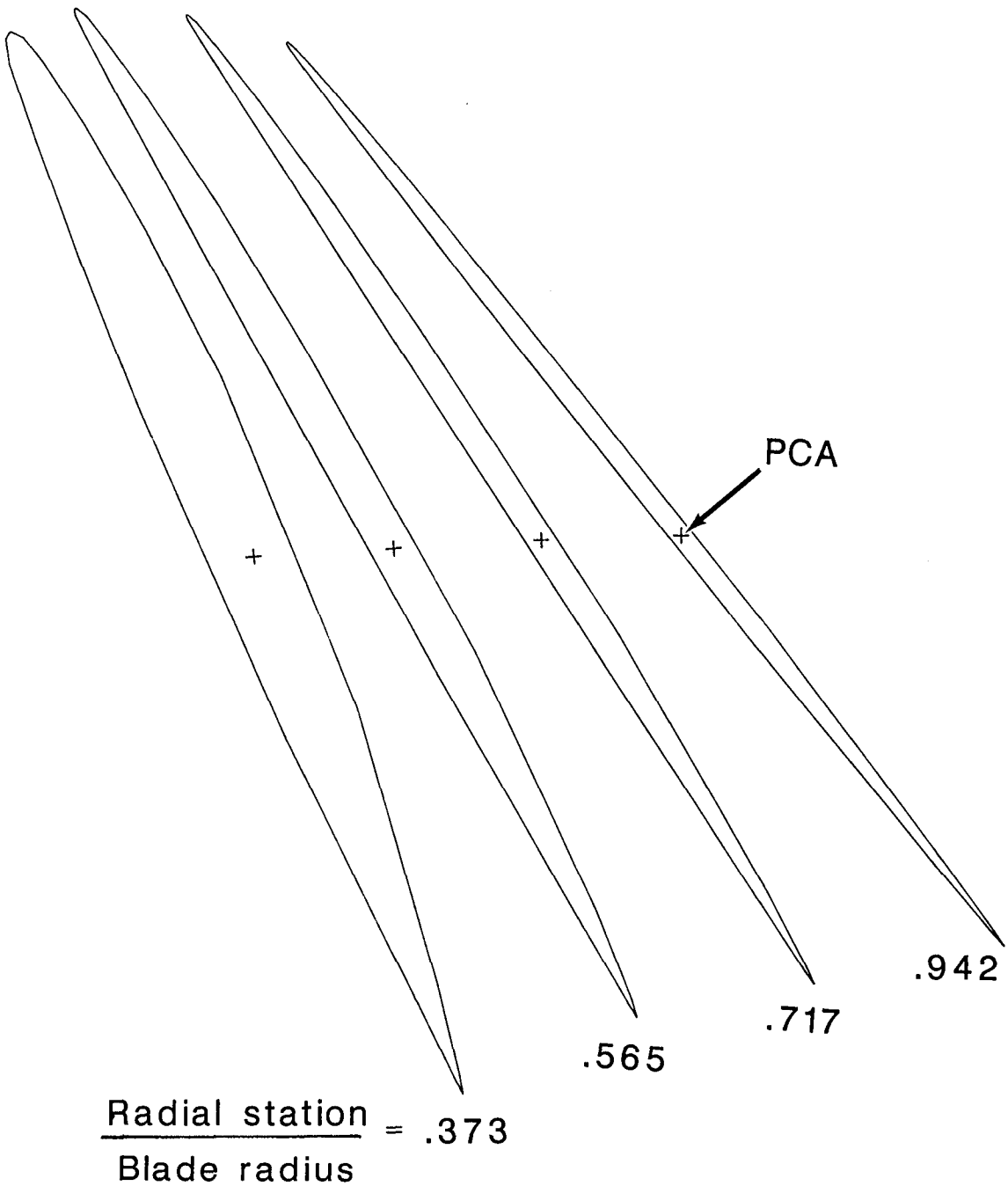

(b) Modified SR-2 airfoil sections.

Figure 3. Concluded.

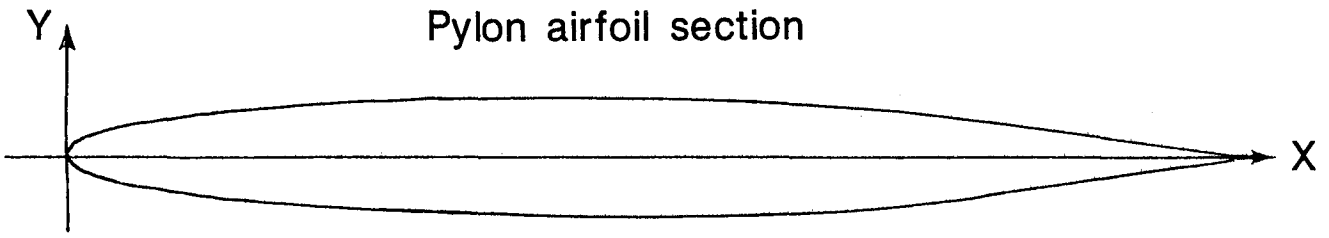

X	Y
0.0	0.0
.0591	.1329
.2356	.2422
.5267	.3349
.9277	.4173
1.4324	.4935
2.0327	.5622
3.4813	.6739
5.1824	.7443
7.0290	.7624
8.9053	.7214
10.6933	.6114
12.2806	.4183
13.5676	.2093
14.4733	.0851
15.0000	.0337

Figure 4. Airfoil section for pusher pylons. X and Y are in inches.

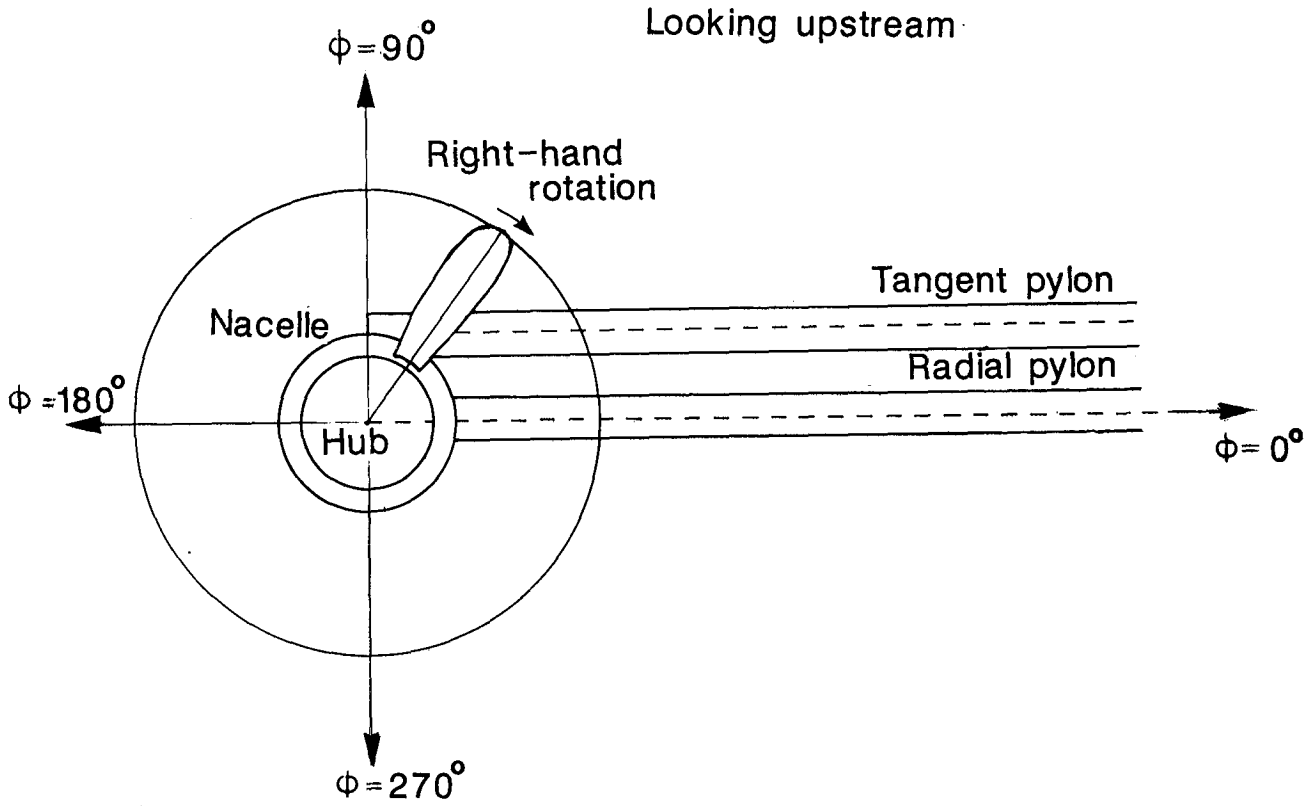

Figure 5. Sketch showing pylon/nacelle attachments for radial pylon and tangent pylon.

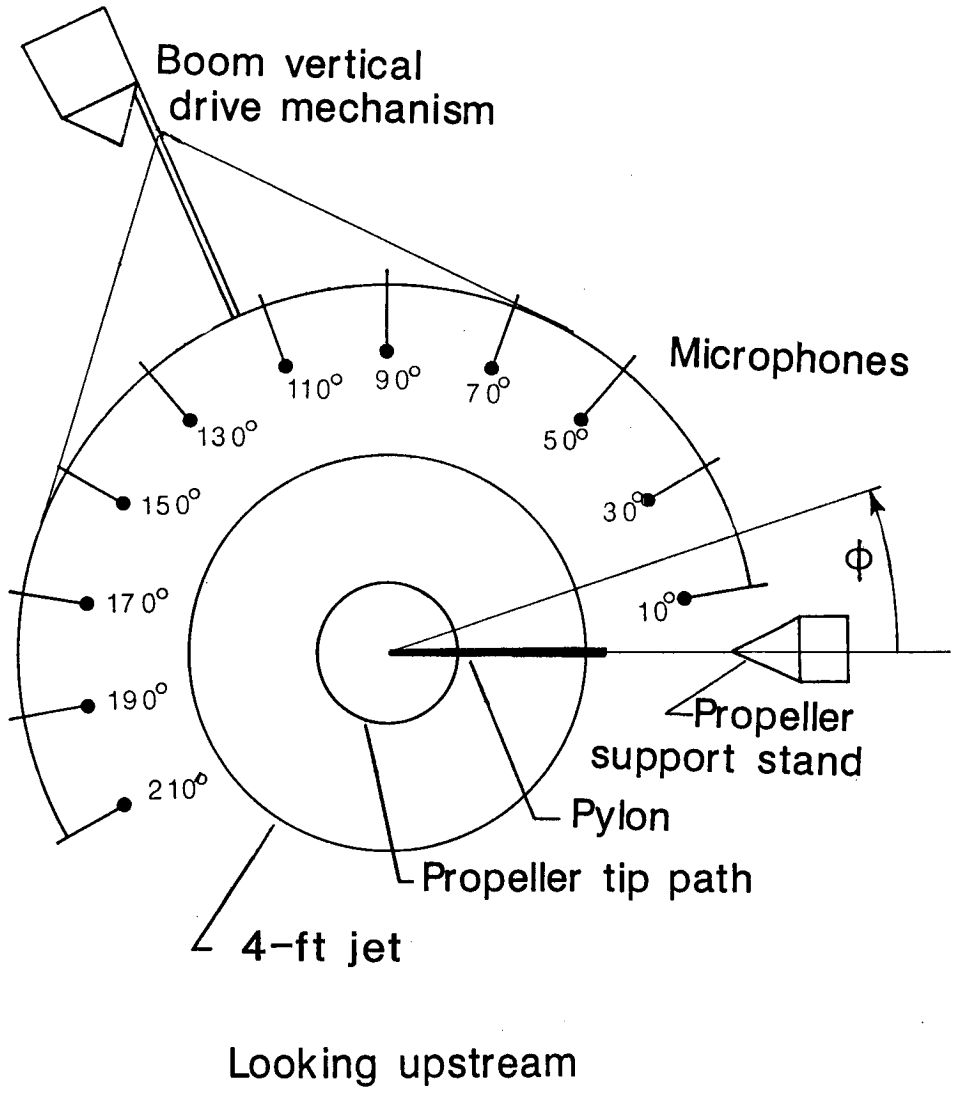

Figure 6. Plan view of far-field microphone measurement array.

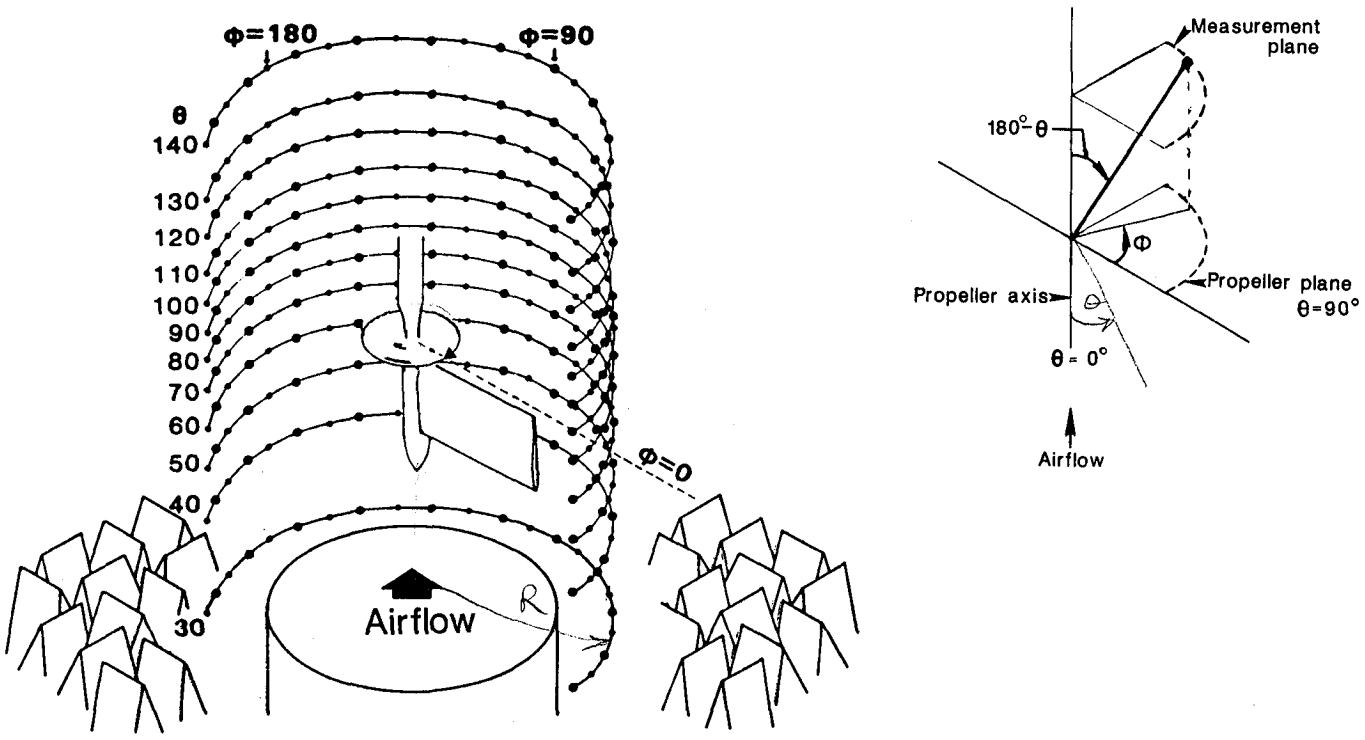

Figure 7. Sketch showing coordinate system and spatial array of measurement locations. ϕ and θ are in degrees.

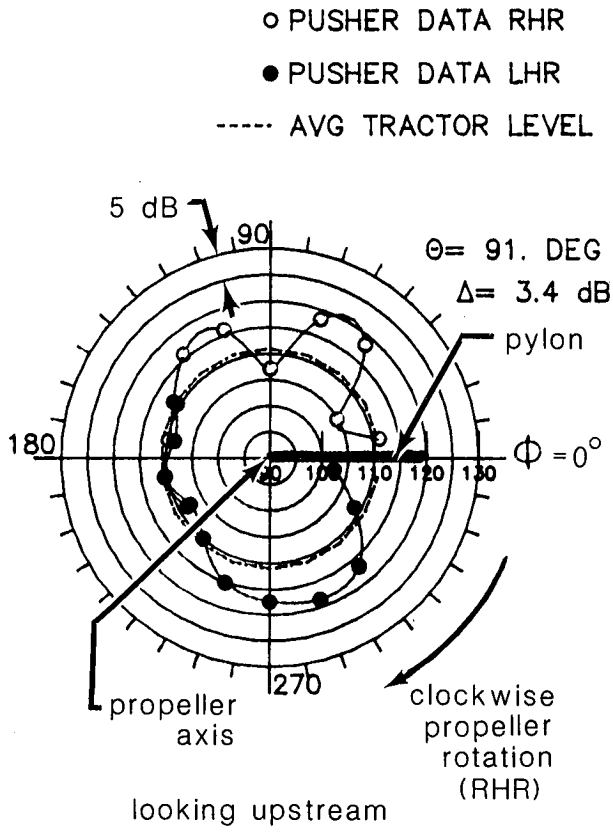

Figure 8. Sample polar plot showing propeller rotation and pylon location. Plotted data are OASPL values in decibels. ϕ and θ are in degrees.

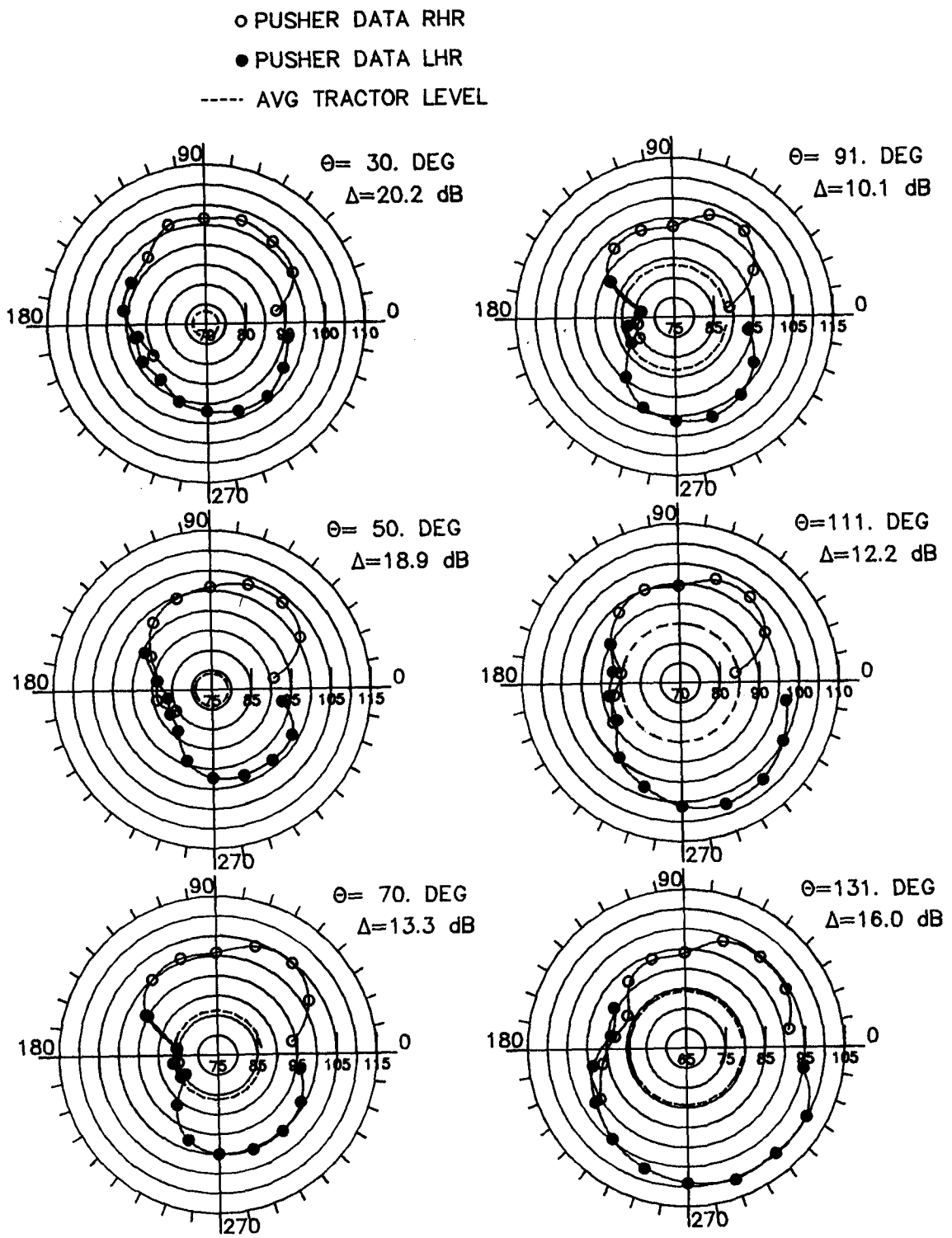

(a) 7200 rpm; $M_T = 0.456$; $(\mathrm{SHP}/d^2)/B = 0.14$ hp/ft^2.

Figure 9. OASPL directivity comparisons for tractor and pusher (0.1c) installations. $\beta_{.75} = 18.8°$; four blades. Plotted data are OASPL values in decibels. Circumferential angles ϕ are in degrees.

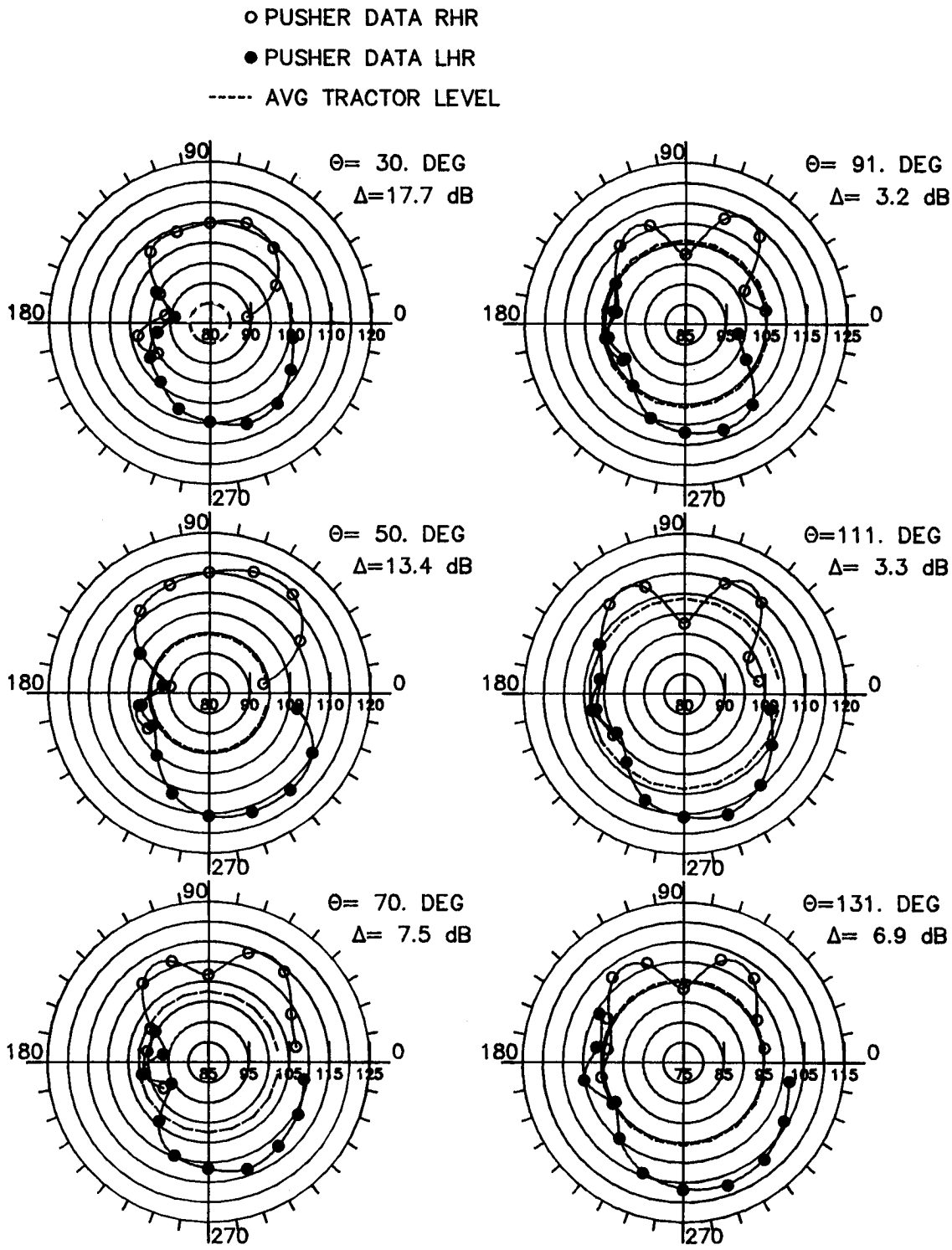

(b) 9500 rpm; $M_T = 0.601$; $(\mathrm{SHP}/d^2)/B = 0.94$ hp/ft^2.

Figure 9. Continued.

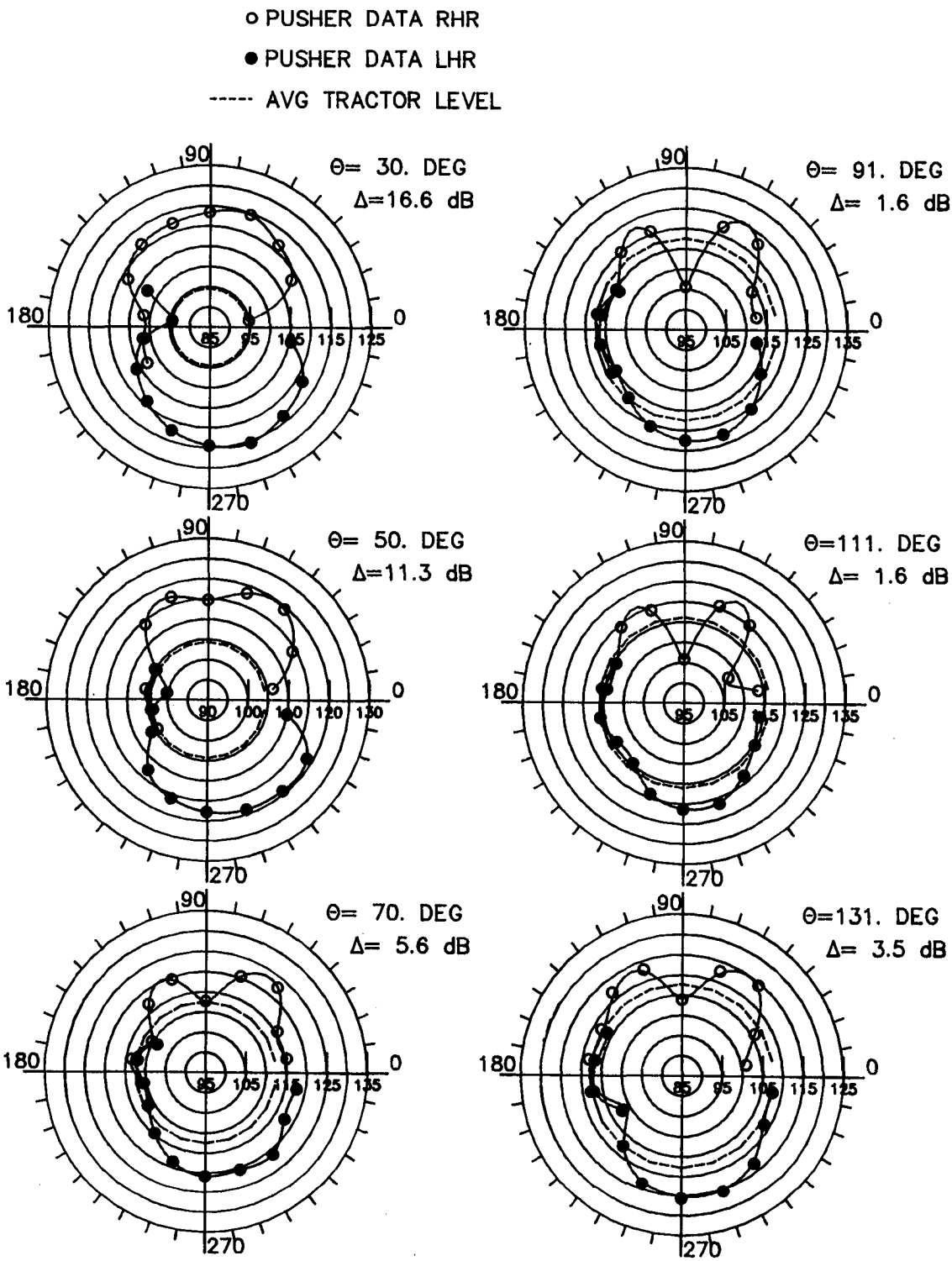

(c) 11 400 rpm; $M_T = 0.722$; $(\mathrm{SHP}/d^2)/B = 2.13$ hp/ft^2.

Figure 9. Concluded.

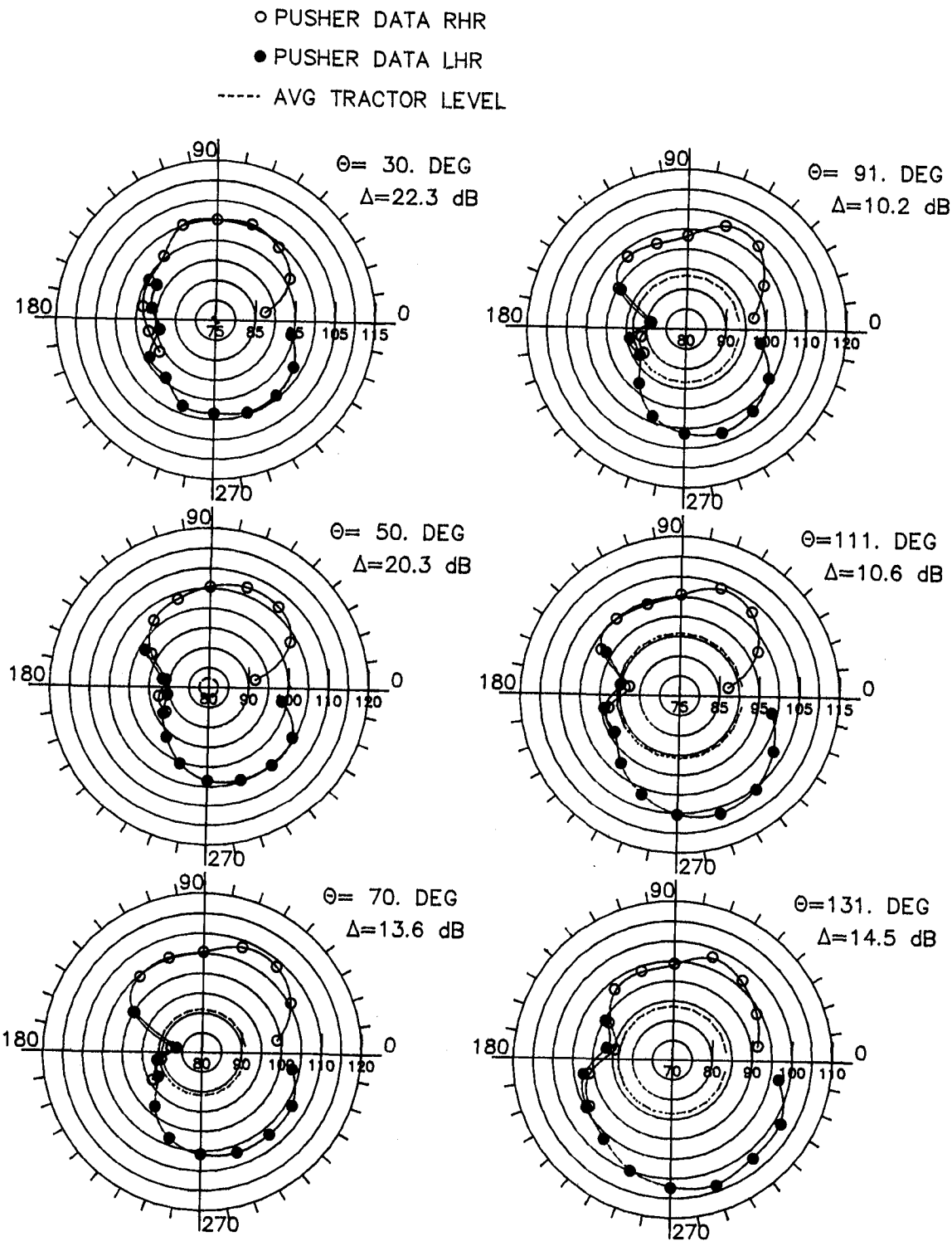

(a) 7200 rpm; $M_T = 0.456$; $(\mathrm{SHP}/d^2)/B = 0.52$ hp/ft^2.

Figure 10. OASPL directivity comparisons for tractor and pusher (0.1c) installations. $\beta_{.75} = 24.0°$; four blades. Plotted data are OASPL values in decibels. Circumferential angles ϕ are in degrees.

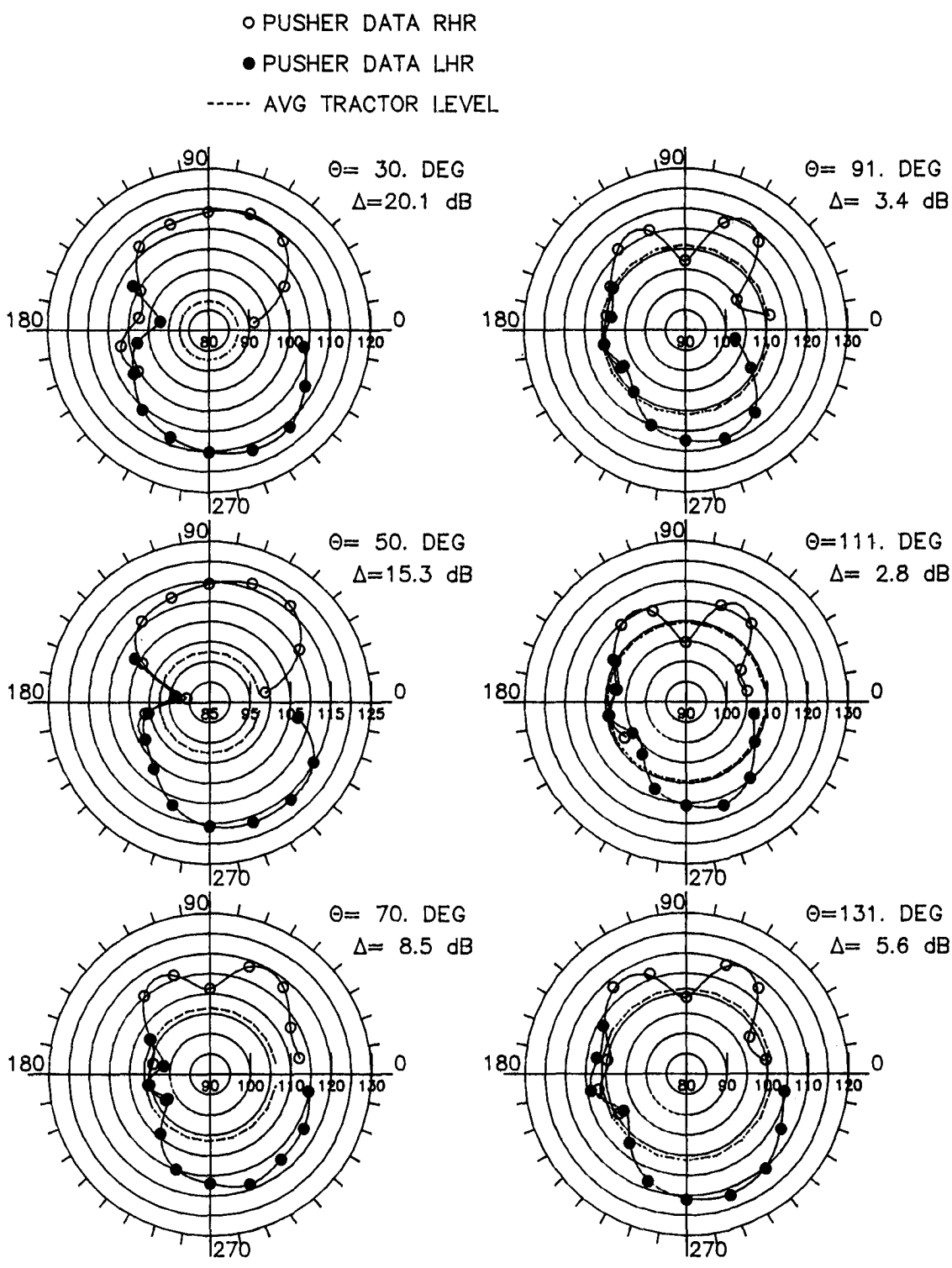

(b) 9500 rpm; $M_T = 0.601$; $(\mathrm{SHP}/d^2)/B = 2.0$ hp/ft^2.

Figure 10. Continued.

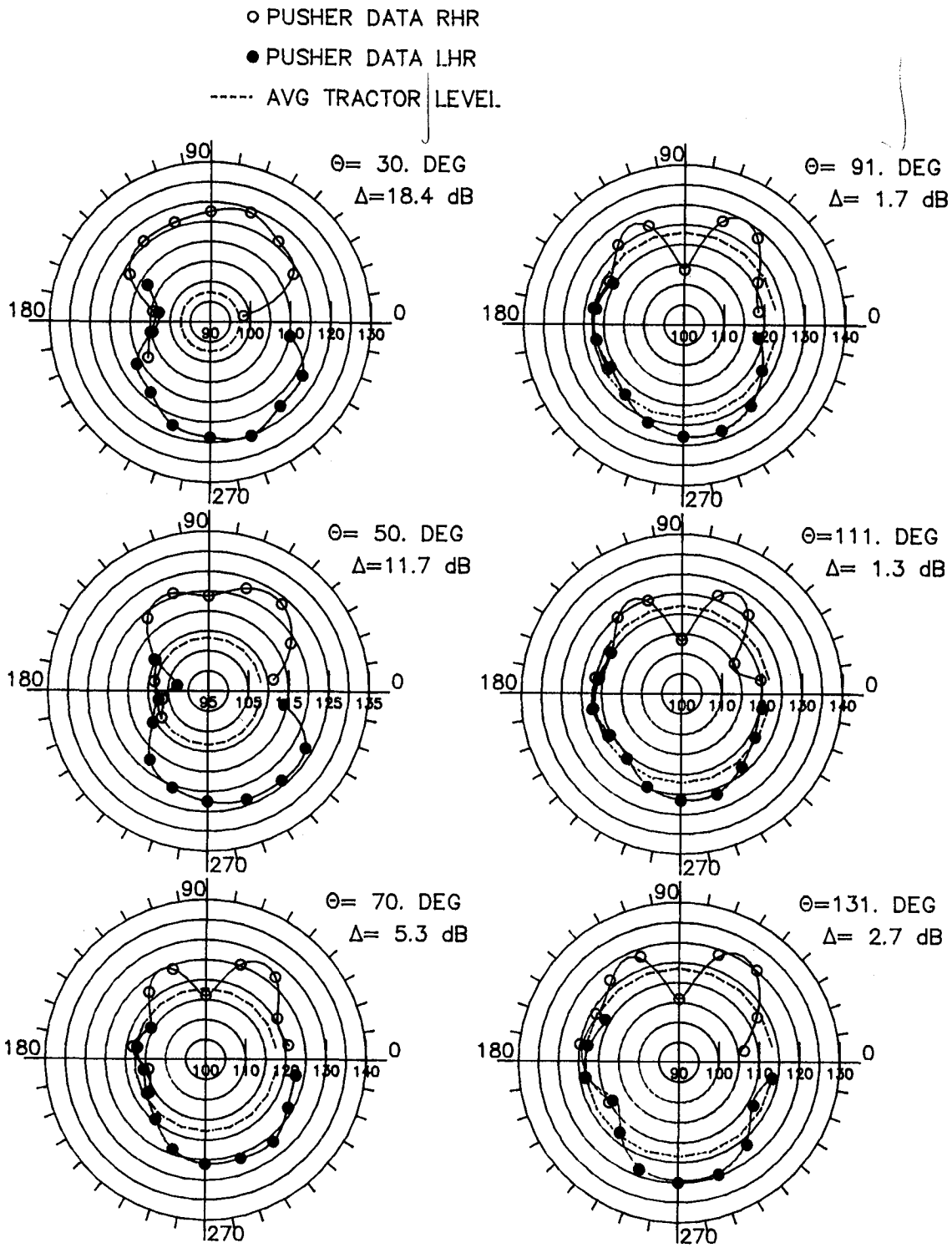

(c) 11 400 rpm; $M_T = 0.722$; $(\mathrm{SHP}/d^2)/B = 4.26$ hp/ft^2.

Figure 10. Concluded.

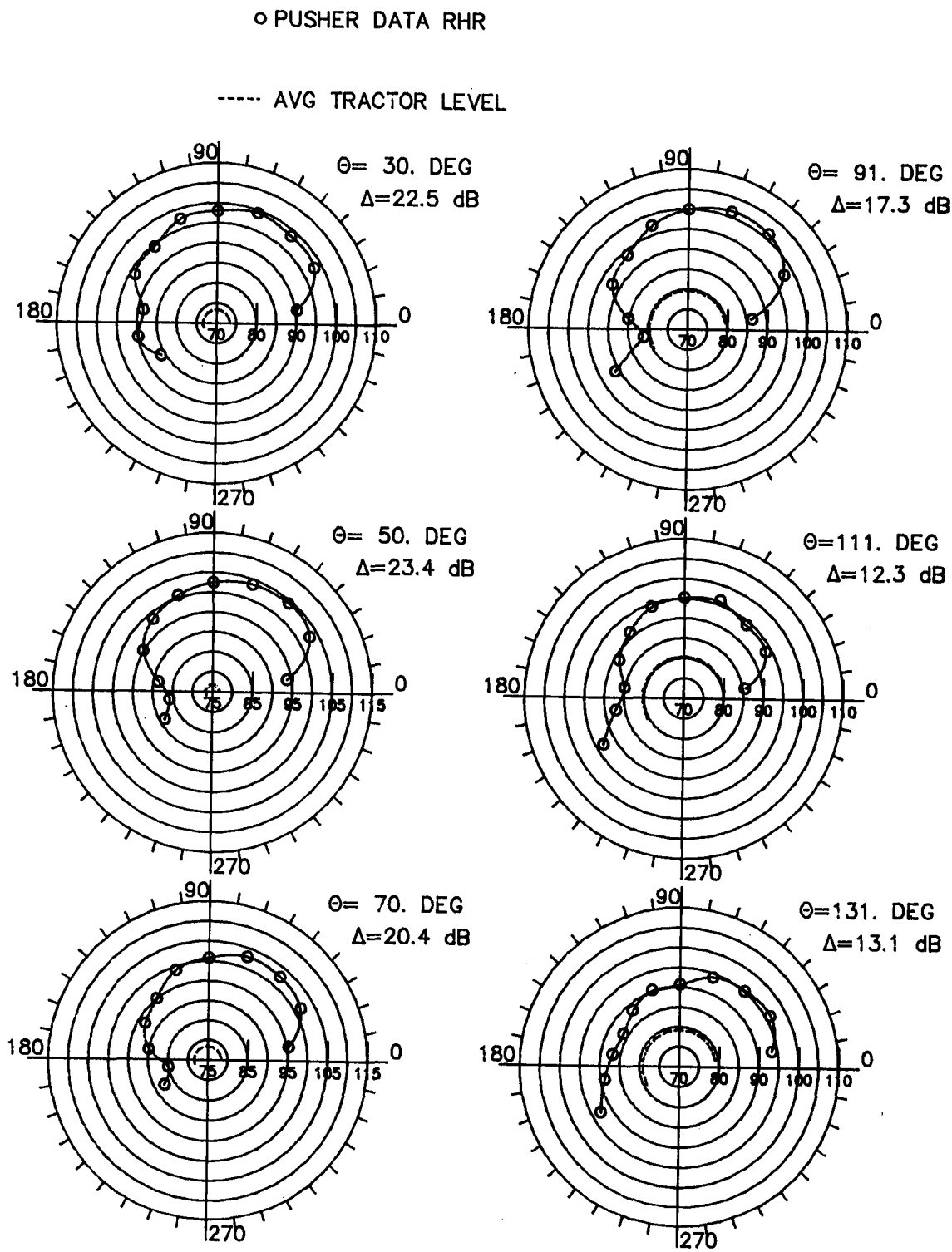

(a) 7200 rpm; $M_T = 0.456$; $(\mathrm{SHP}/d^2)/B = 0.12$ hp/ft^2.

Figure 11. OASPL directivity comparisons for tractor and pusher ($0.1c$) installations. $\beta_{.75} = 20.0°$; eight blades. Plotted data are OASPL values in decibels. Circumferential angles ϕ are in degrees.

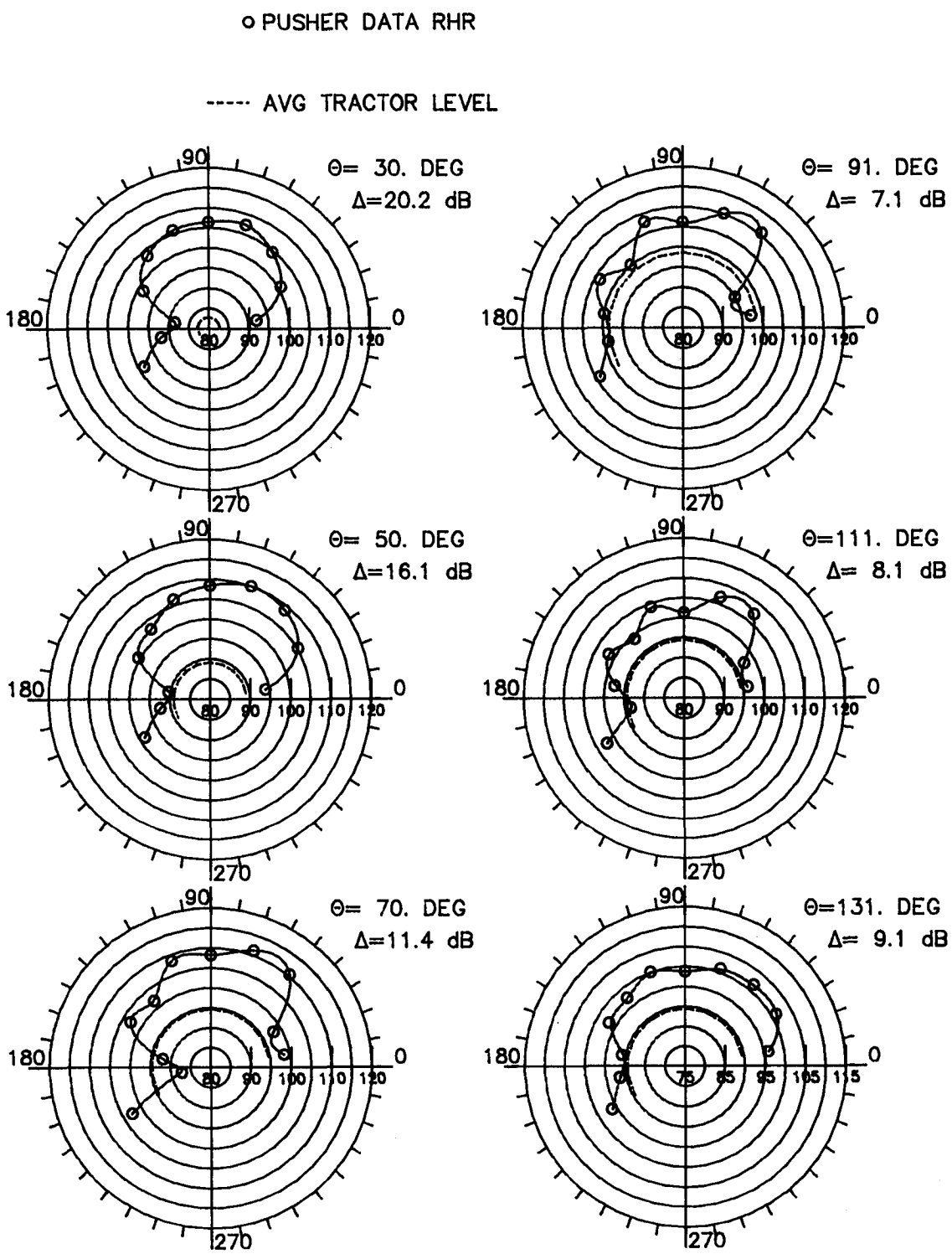

(b) 9500 rpm; $M_T = 0.601$; $(\mathrm{SHP}/d^2)/B = 0.73$ hp/ft^2.

Figure 11. Continued.

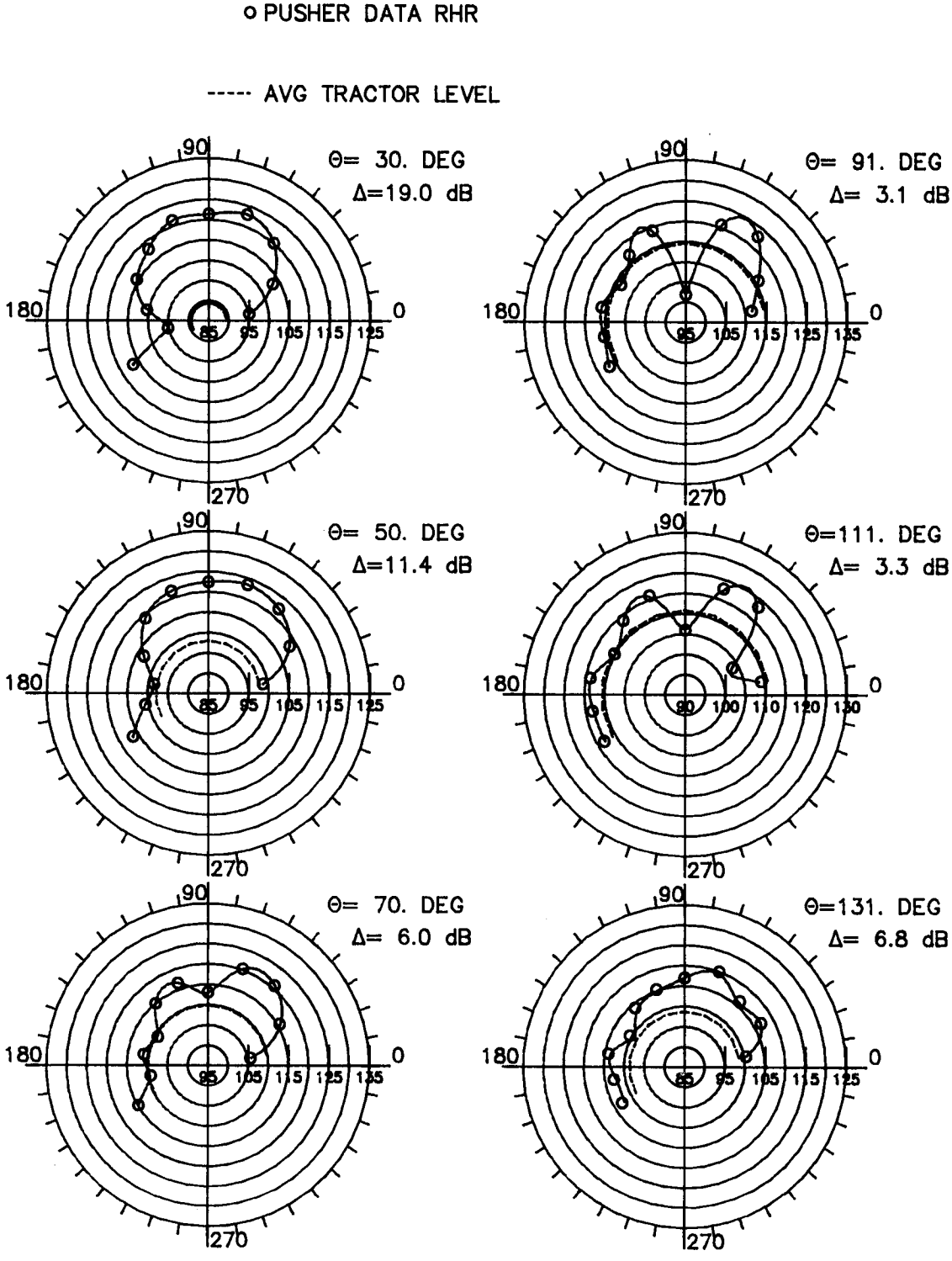

(c) 11 400 rpm; $M_T = 0.7222$; $(\mathrm{SHP}/d^2)/B = 1.61$ hp/ft^2.

Figure 11. Concluded.

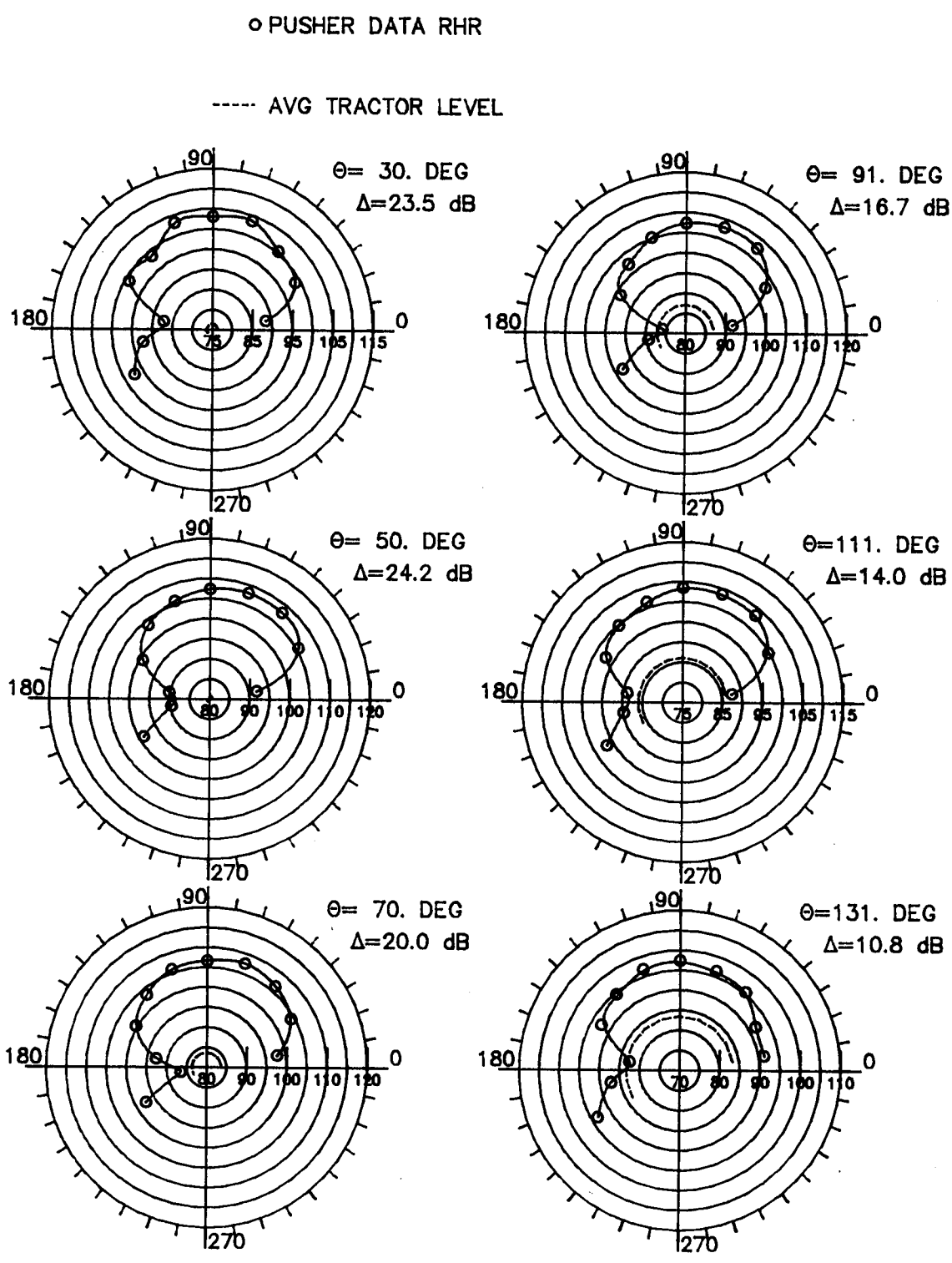

Figure 12. OASPL directivity comparisons for tractor and pusher (0.1c) installations. $\beta_{.75} = 30.0°$; eight blades; 7200 rpm; $M_T = 0.456$; $(\mathrm{SHP}/d^2)/B = 1.0$ hp/ft^2. Plotted data are OASPL values in decibels. Circumferential angles ϕ are in degrees.

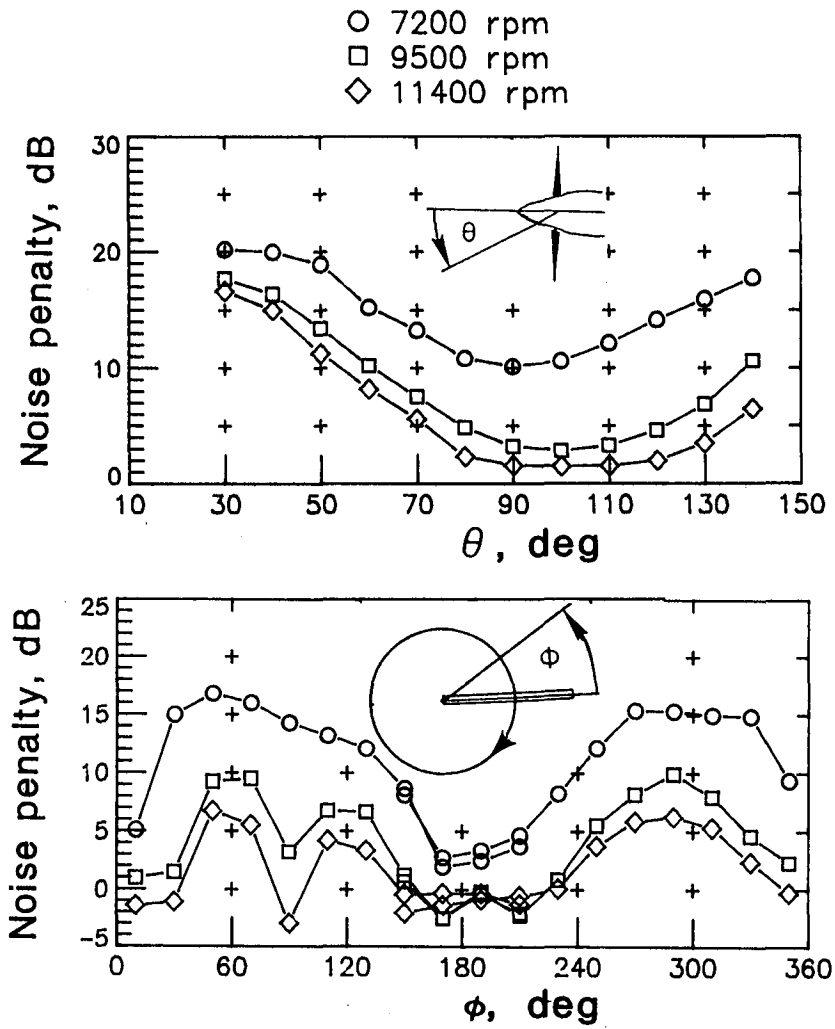

Figure 13. Variation of noise penalty for pusher configuration with θ and ϕ. $\beta_{.75} = 18.8°$; four blades.

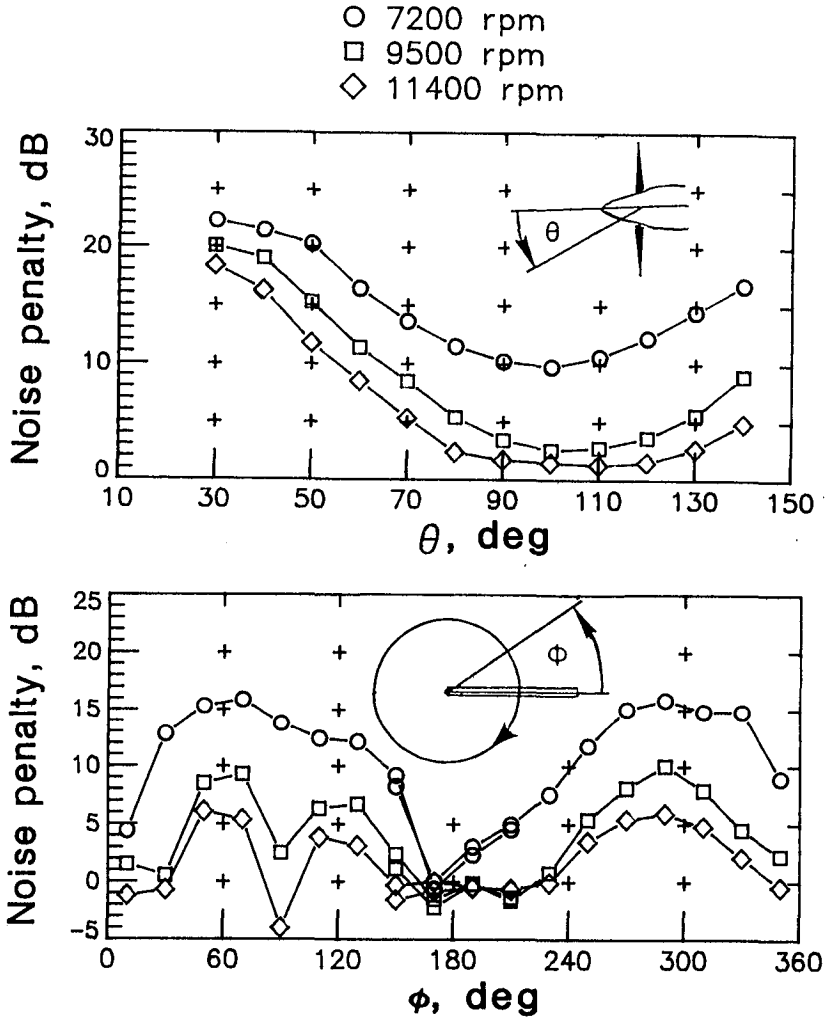

Figure 14. Variation of noise penalty for pusher configuration with θ and ϕ. $\beta_{.75} = 24.0°$; four blades.

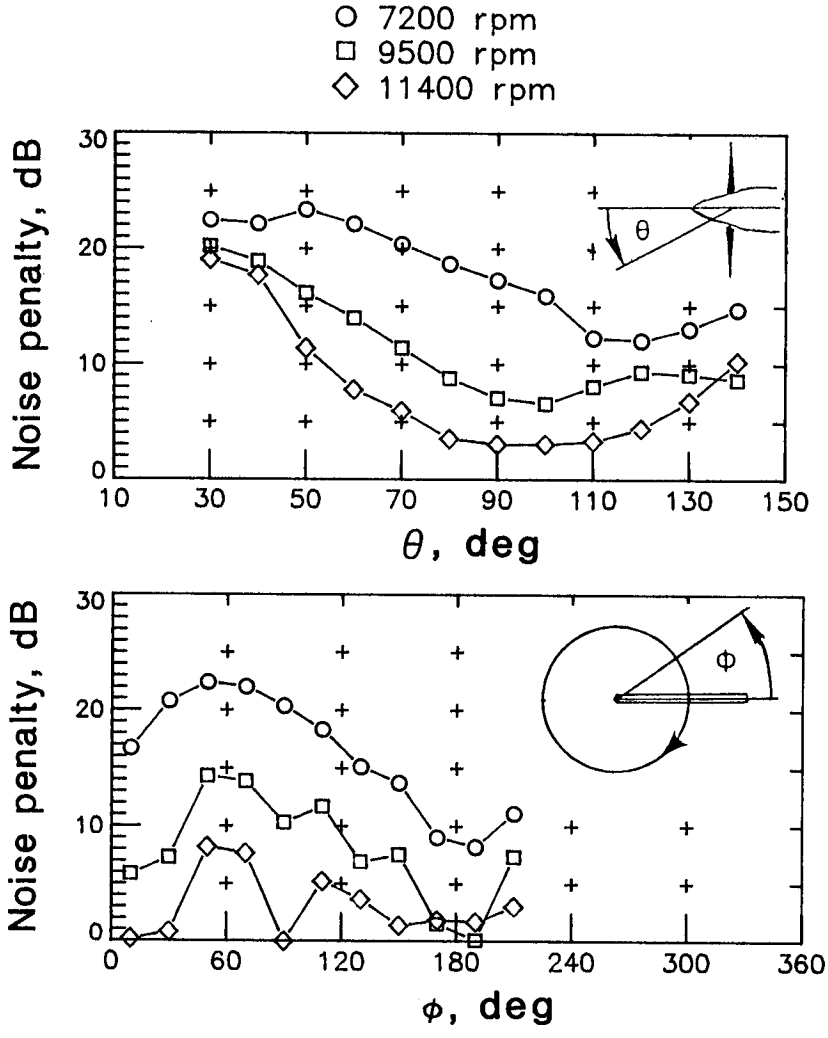

Figure 15. Variation of noise penalty for pusher configuration with θ and ϕ. $\beta_{.75} = 20.0°$; eight blades.

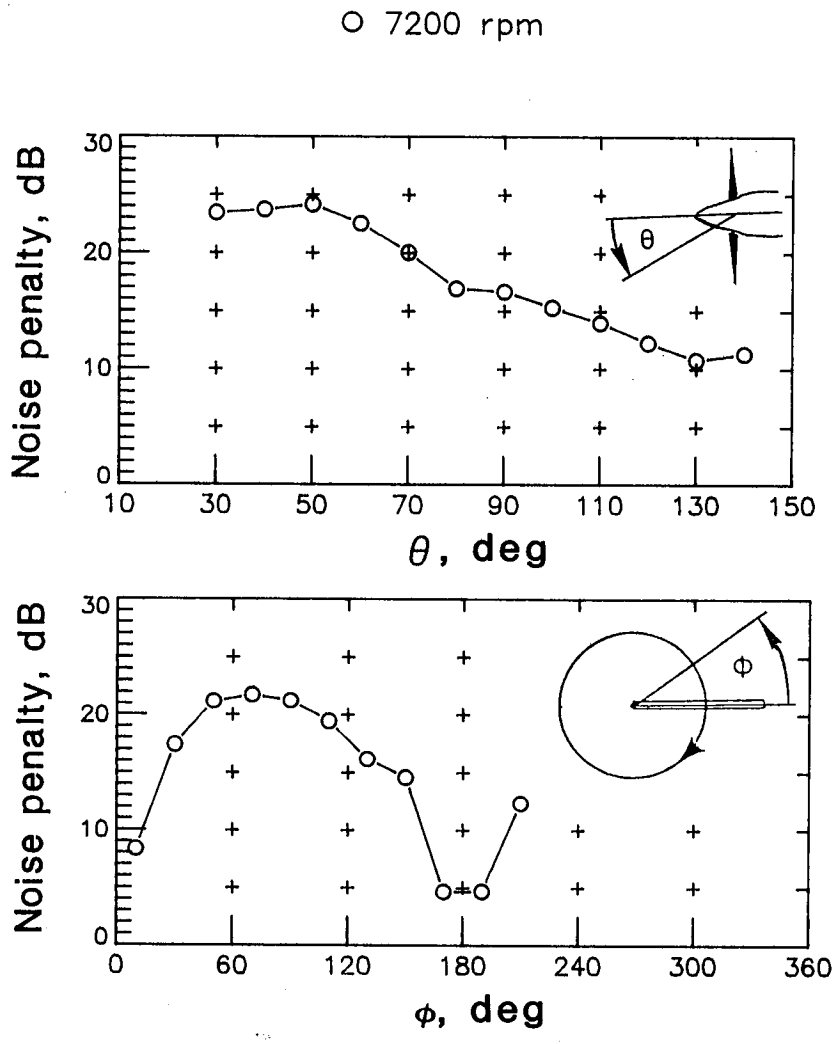

Figure 16. Variation of noise penalty for pusher configuration with θ and ϕ. $\beta_{.75} = 30.0°$; eight blades.

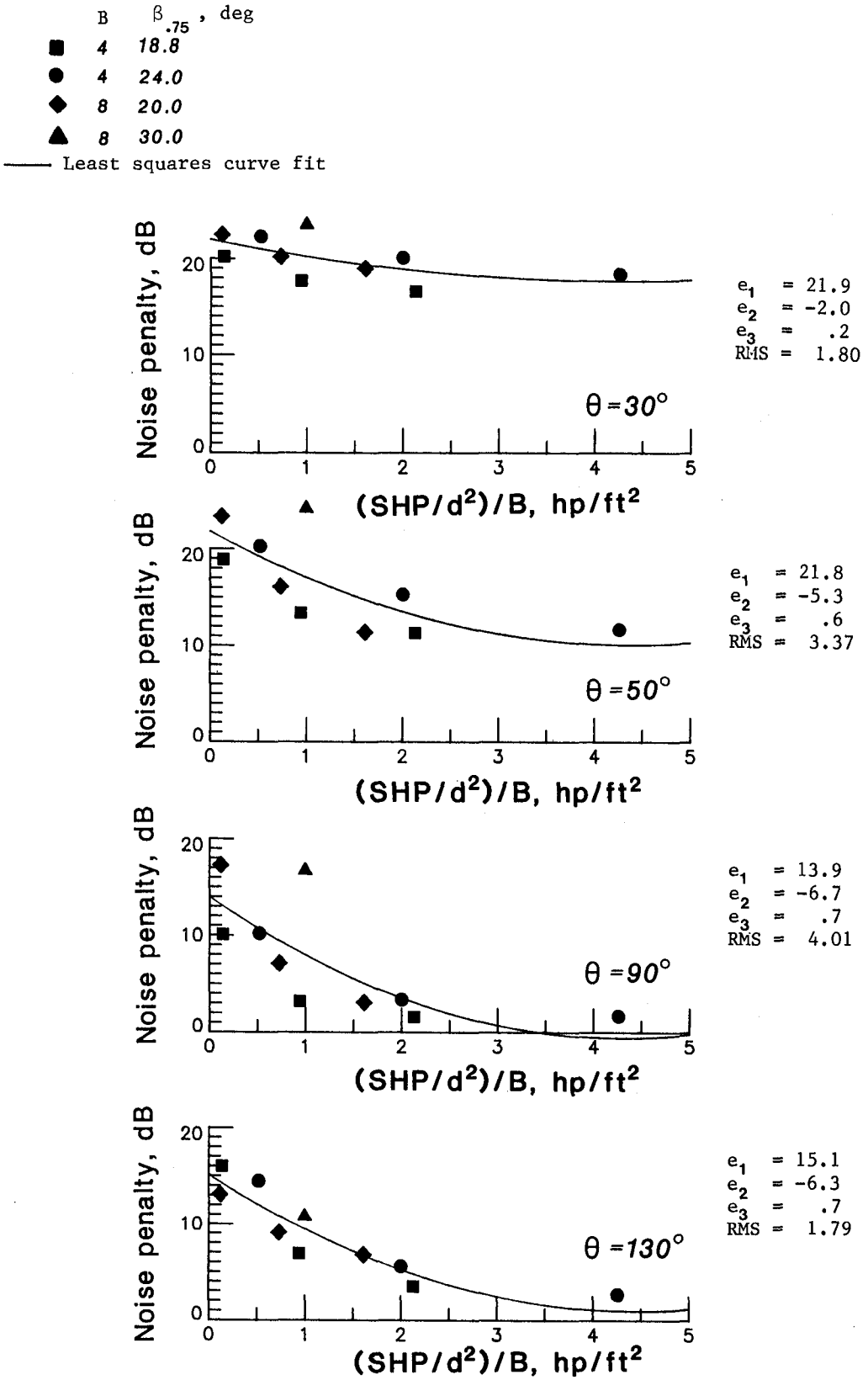

Figure 17. Trends in noise penalty for pusher configuration with $(SHP/d^2)/B$ at selected values of θ.

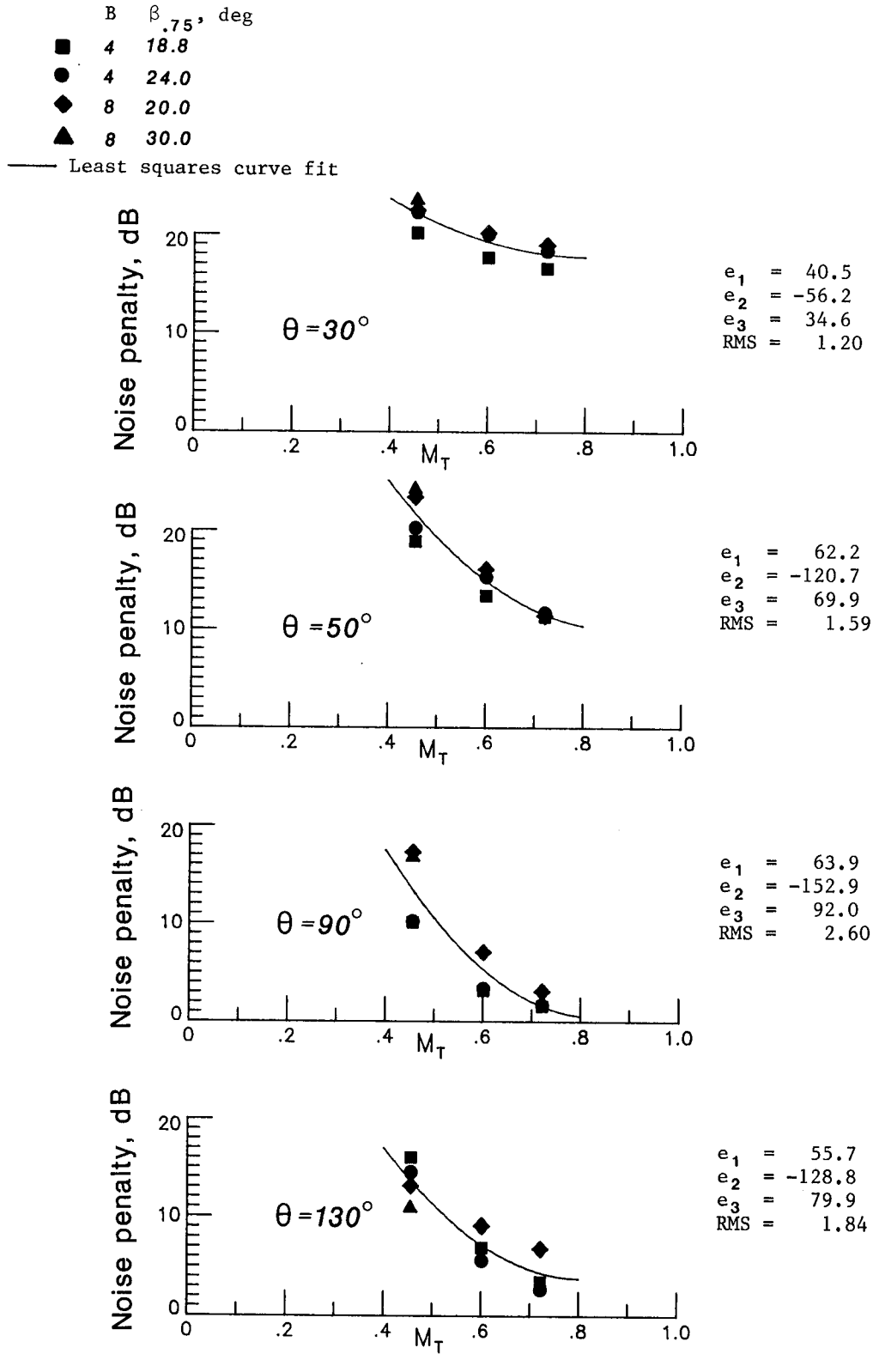

Figure 18. Trends in noise penalty for pusher configuration with M_T at selected values of θ.

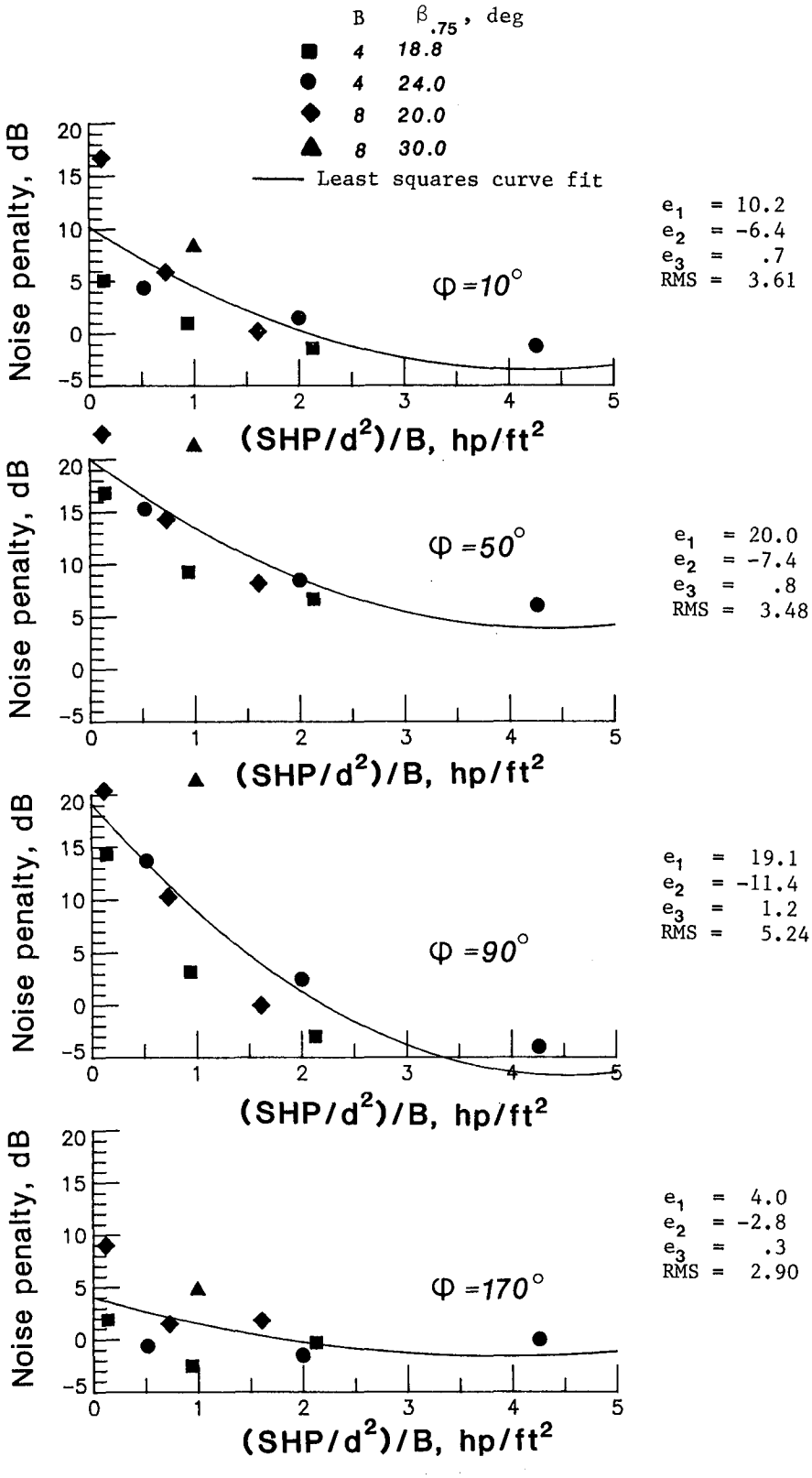

Figure 19. Trends in noise penalty for pusher configuration with $(\mathrm{SHP}/d^2)/B$ at selected values of ϕ.

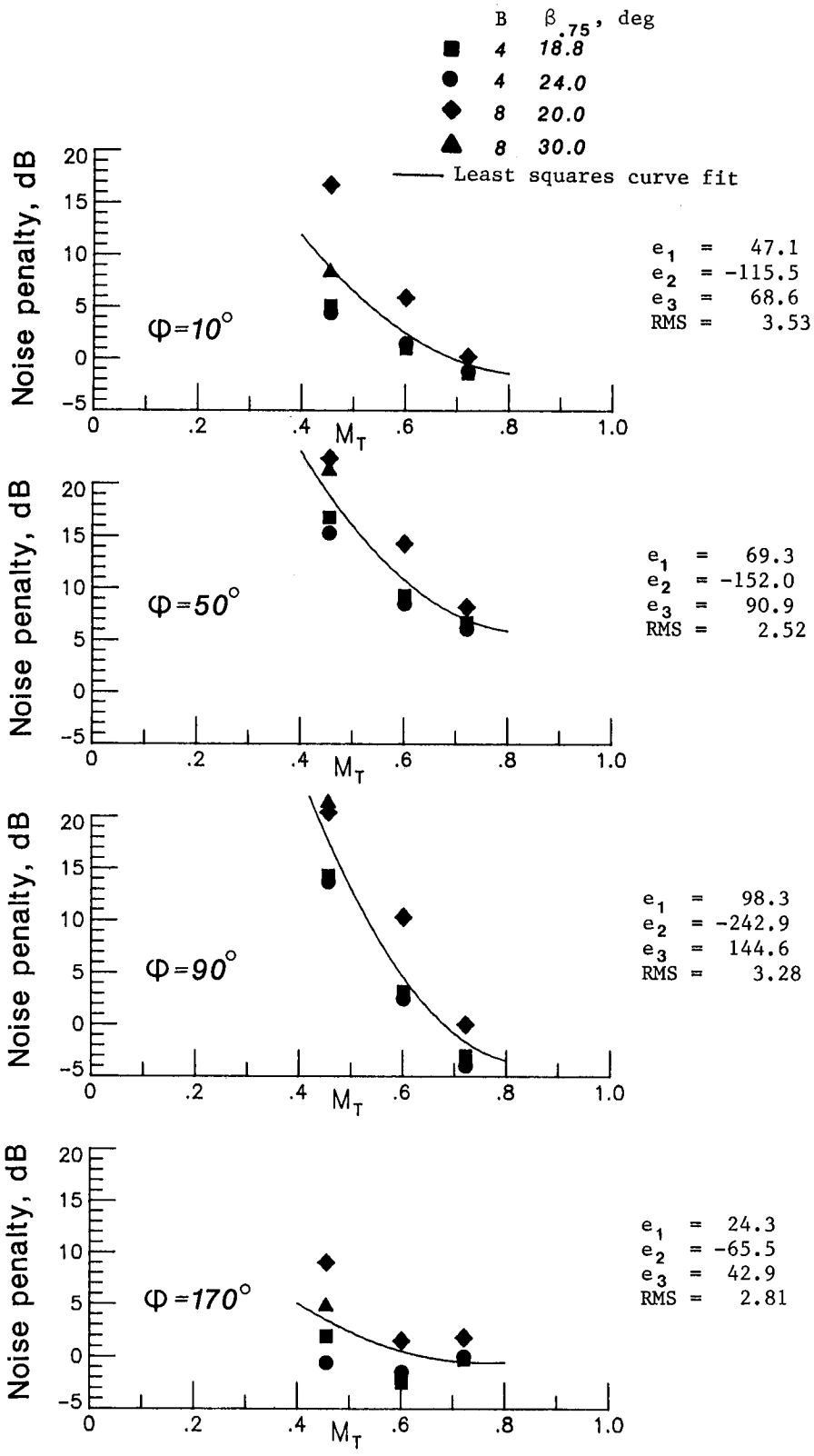

Figure 20. Trends in noise penalty for pusher configuration with M_T at selected values of ϕ.

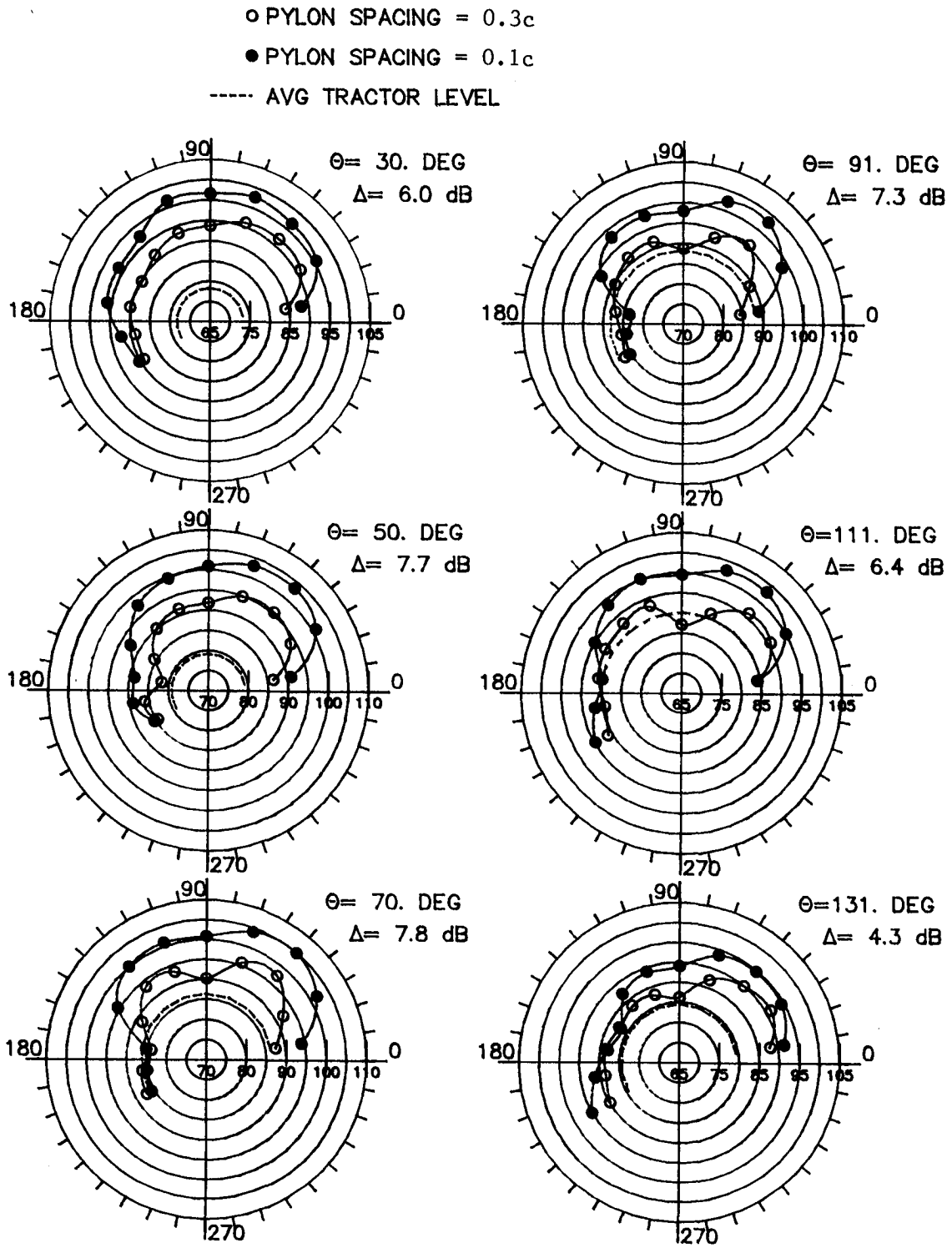

(a) 7200 rpm; $M_T = 0.456$; $(\mathrm{SHP}/d^2)/B = 0.14$ hp/ft^2.

Figure 21. OASPL directivity comparisons for $0.1c$ and $0.3c$ spacing of radial pylon. $\beta_{.75} = 18.8°$; four blades. Plotted data are OASPL values in decibels. Circumferential angles ϕ are in degrees.

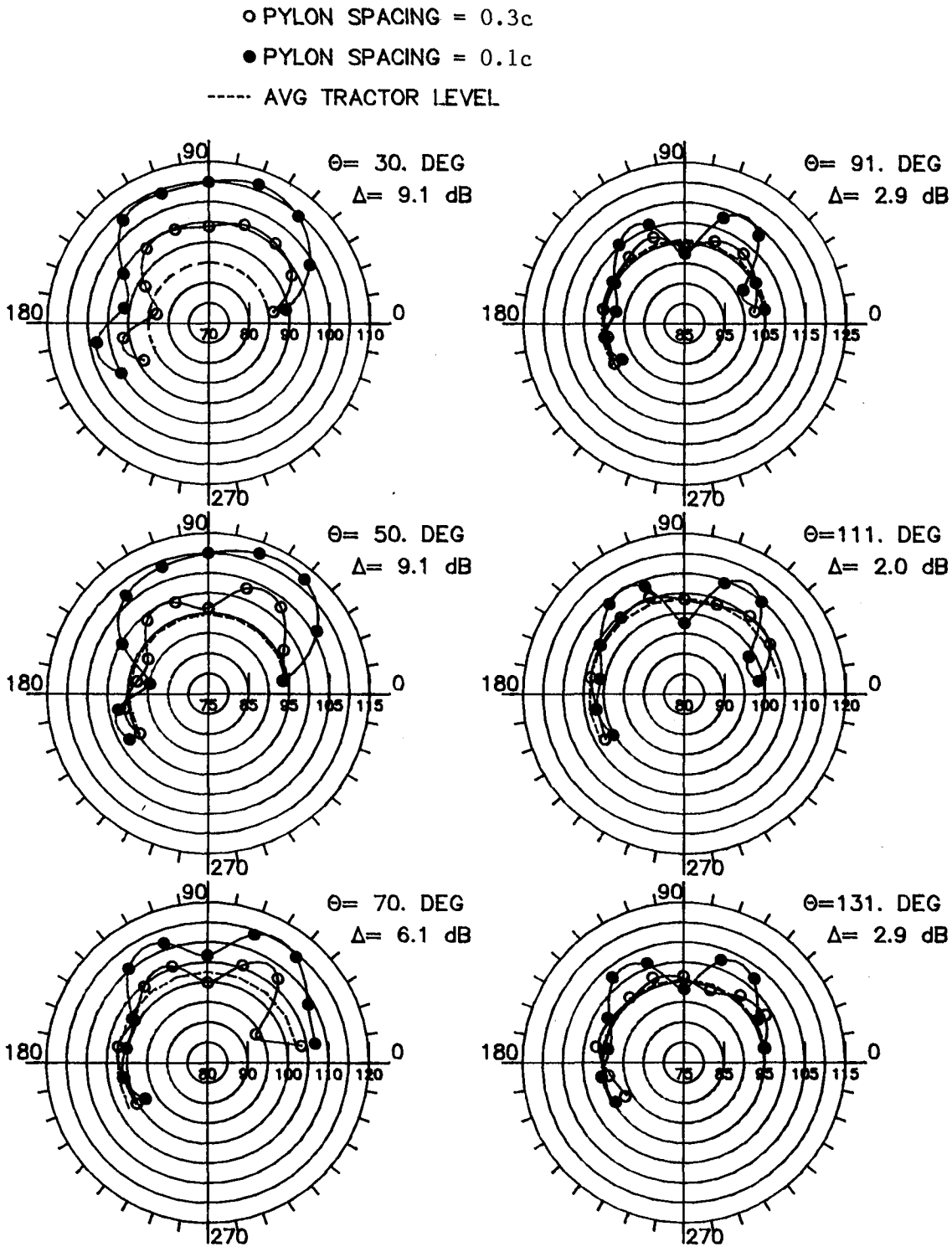

(b) 9500 rpm; $M_T = 0.601$; $(\mathrm{SHP}/d^2)/B = 0.94$ hp/ft^2.

Figure 21. Continued.

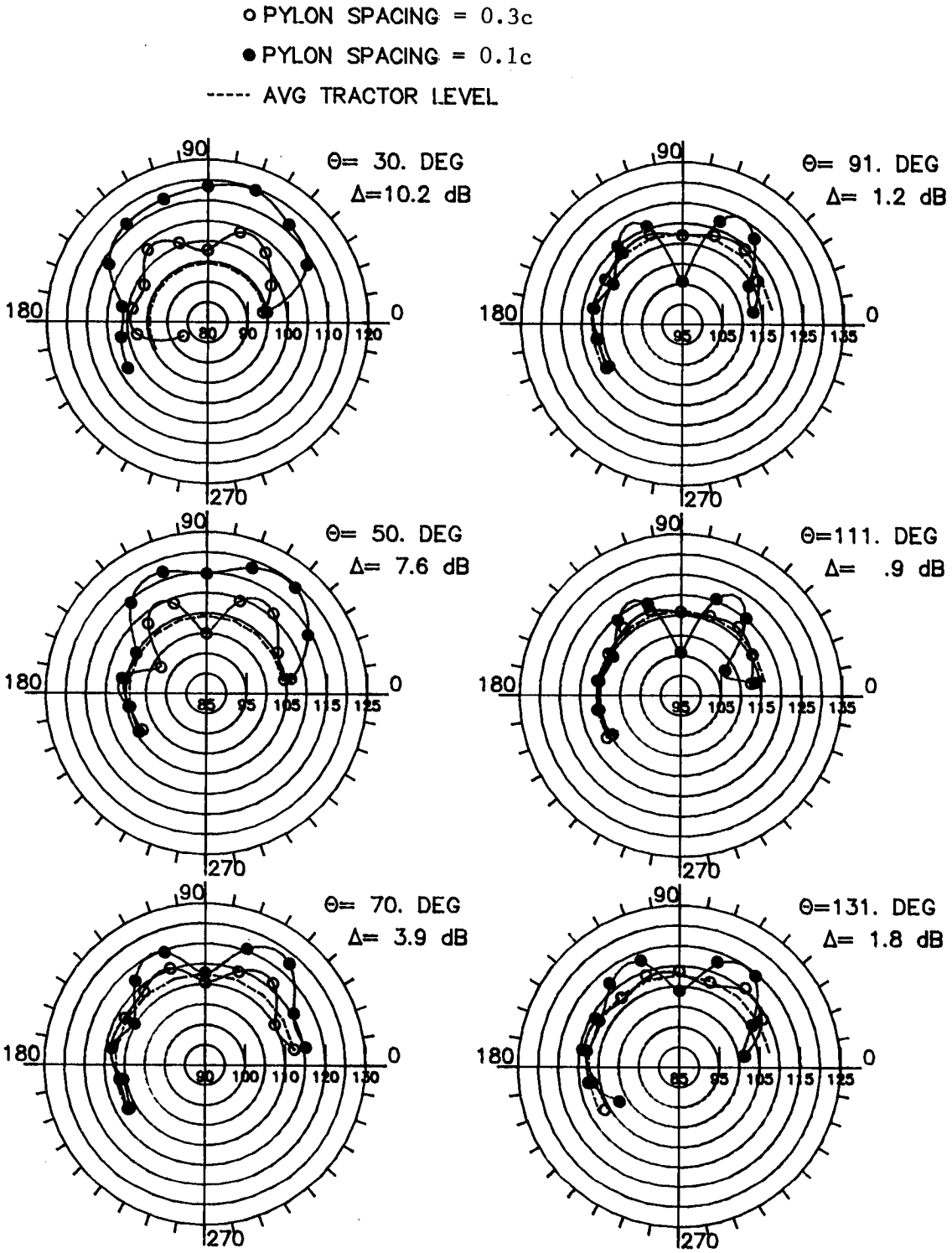

(c) 11 400 rpm; $M_T = 0.722$; $(\mathrm{SHP}/d^2)/B = 2.13$ hp/ft^2.

Figure 21. Concluded.

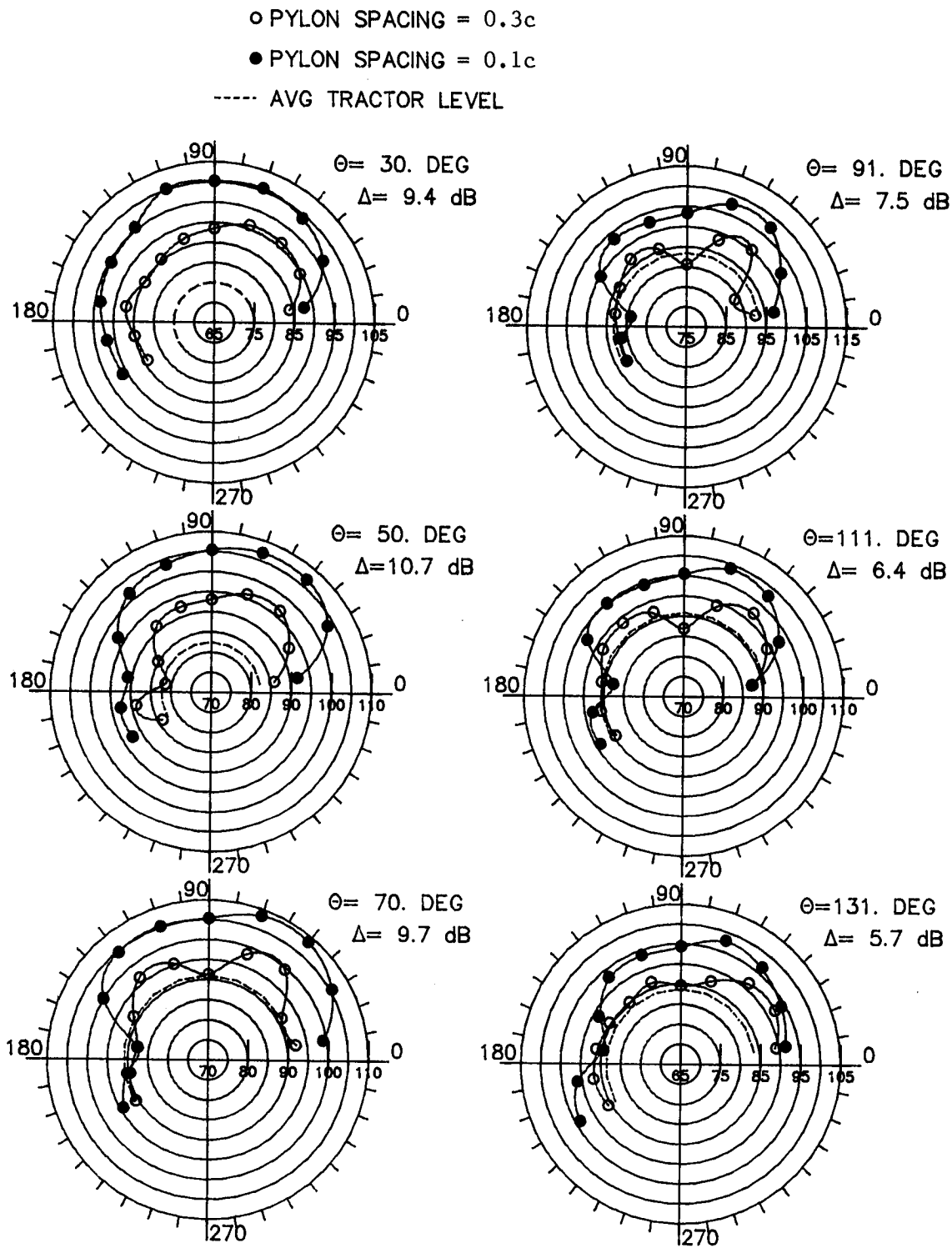

(a) 7200 rpm; $M_T = 0.456$; $(\mathrm{SHP}/d^2)/B = 0.52$ hp/ft^2.

Figure 22. OASPL directivity comparisons for $0.1c$ and $0.3c$ spacing of radial pylon. $\beta_{.75} = 24.0°$; four blades.

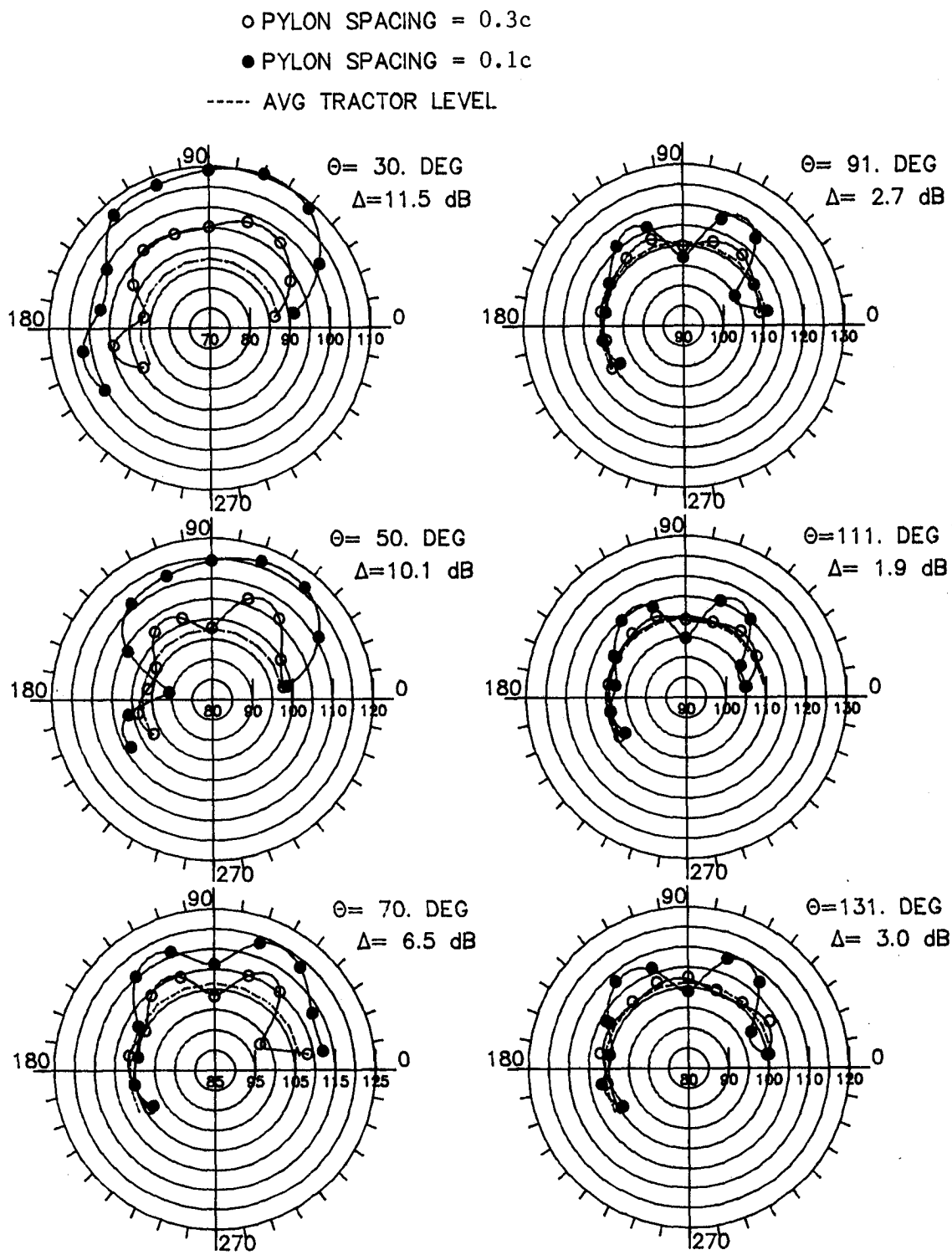

(b) 9500 rpm; $M_T = 0.601$; $(\mathrm{SHP}/d^2)/B = 2.0$ hp/ft^2.

Figure 22. Continued.

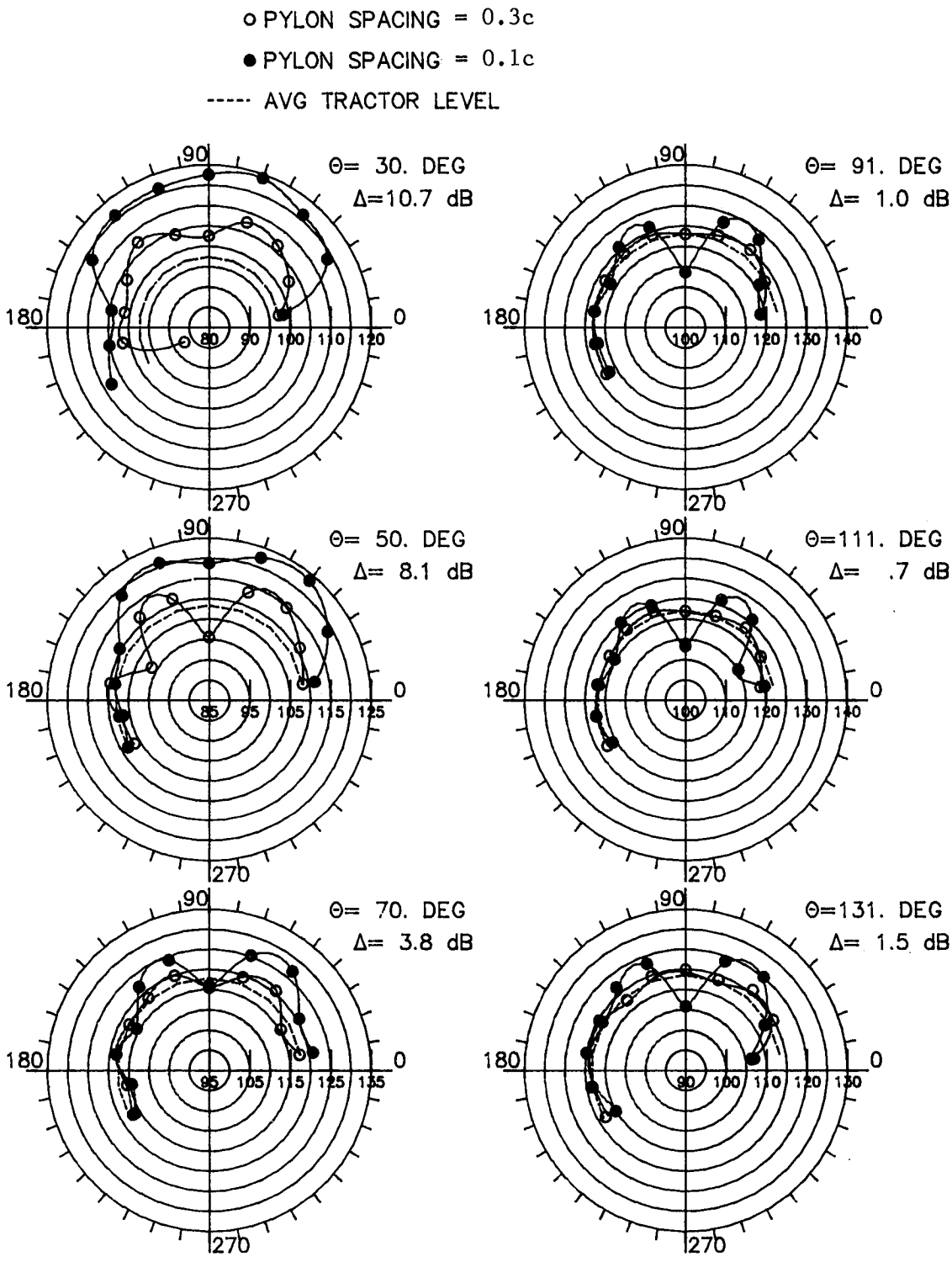

(c) 11 400 rpm; $M_T = 0.722$; $(\mathrm{SHP}/d^2)/B = 4.26$ hp/ft^2.

Figure 22. Concluded.

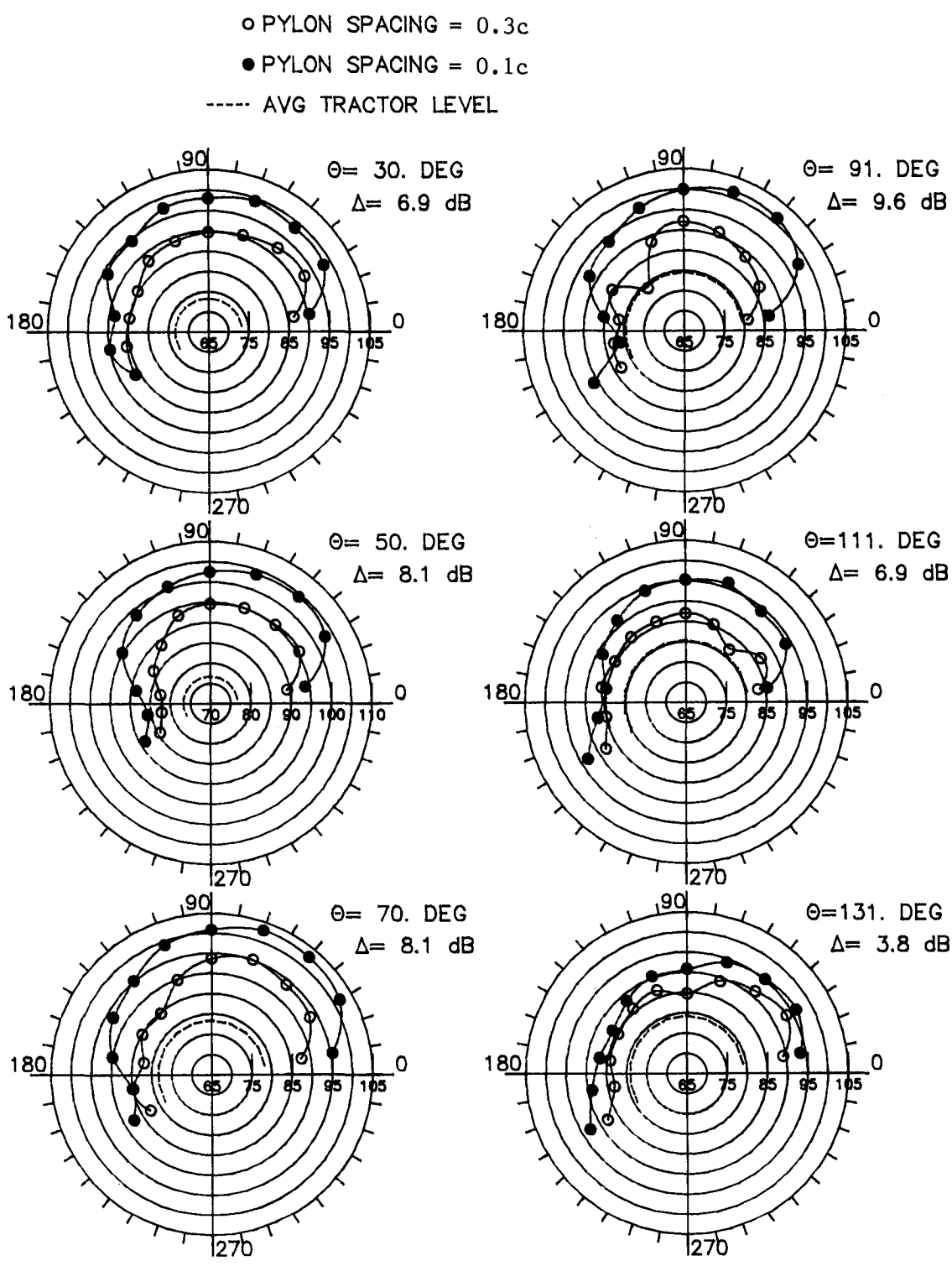

(a) 7200 rpm; $M_T = 0.456$; $(\mathrm{SHP}/d^2)/B = 0.12$ hp/ft^2.

Figure 23. OASPL directivity comparisons for $0.1c$ and $0.3c$ spacing of radial pylon. $\beta_{.75} = 20.0°$; eight blades. Plotted data are OASPL values in decibels. Circumferential angles ϕ are in degrees.

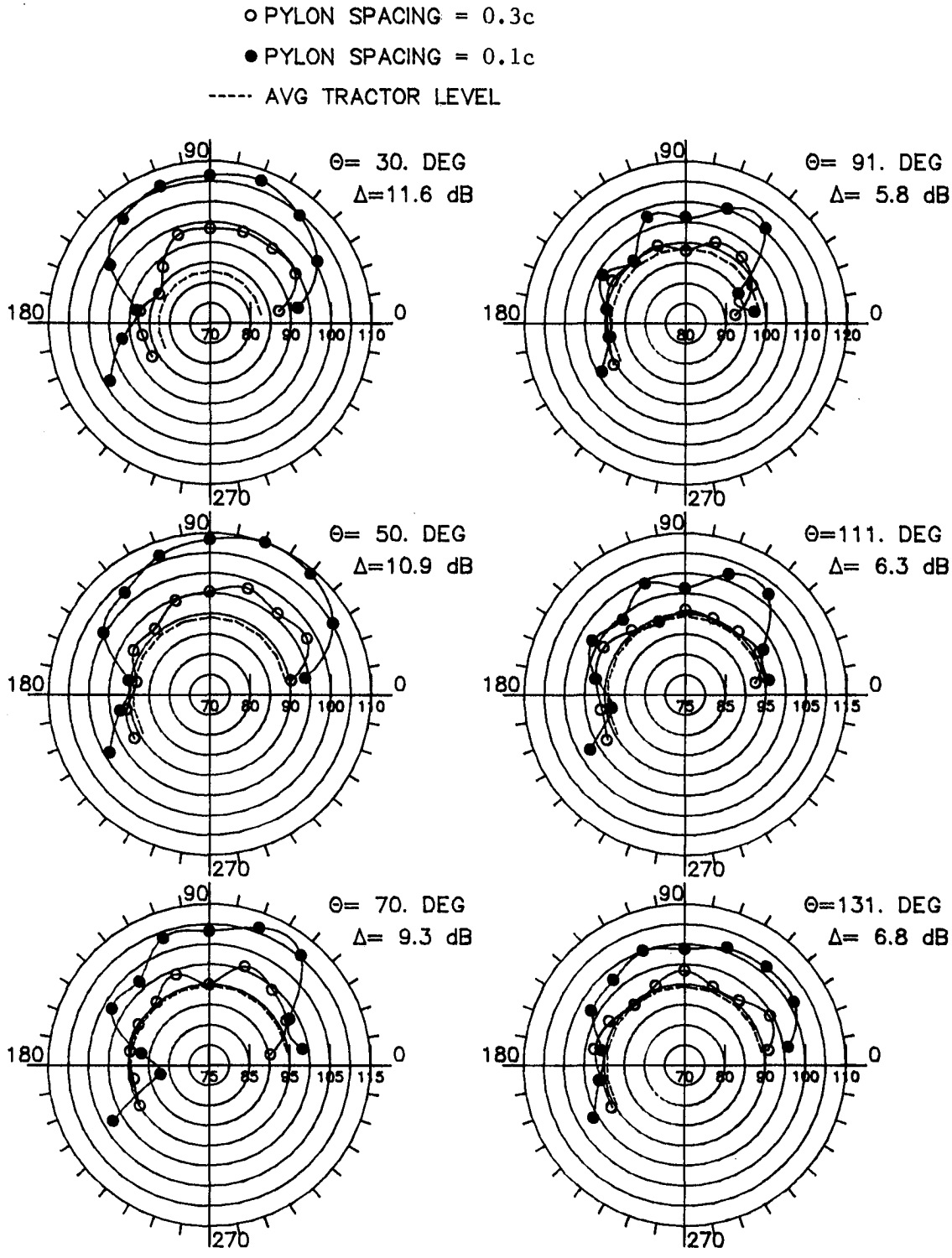

(b) 9500 rpm; $M_T = 0.601$; $(\mathrm{SHP}/d^2)/B = 0.73$ hp/ft^2.

Figure 23. Continued.

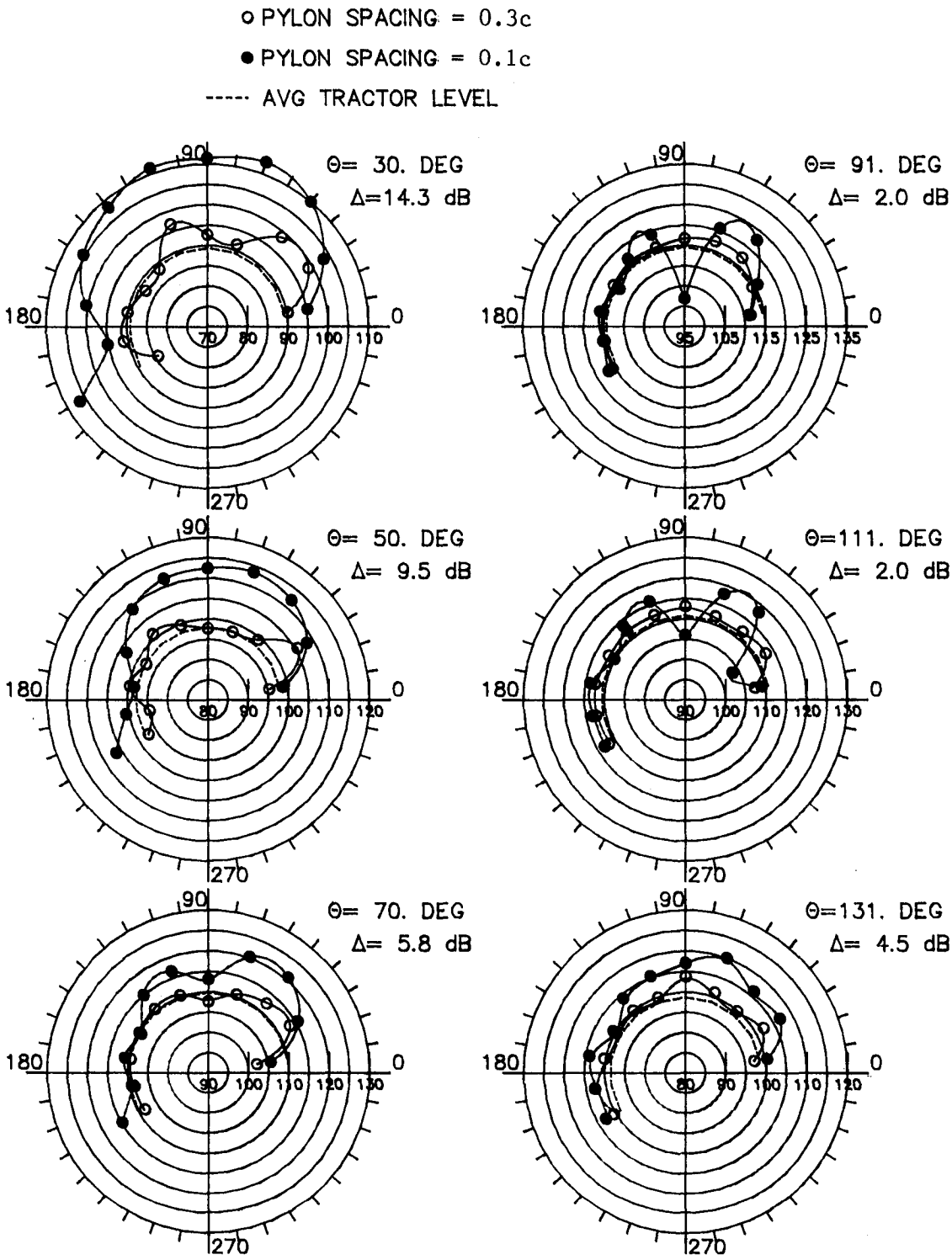

(c) 11 400 rpm; $M_T = 0.722$; $(\mathrm{SHP}/d^2)/B = 1.61$ hp/ft^2.

Figure 23. Concluded.

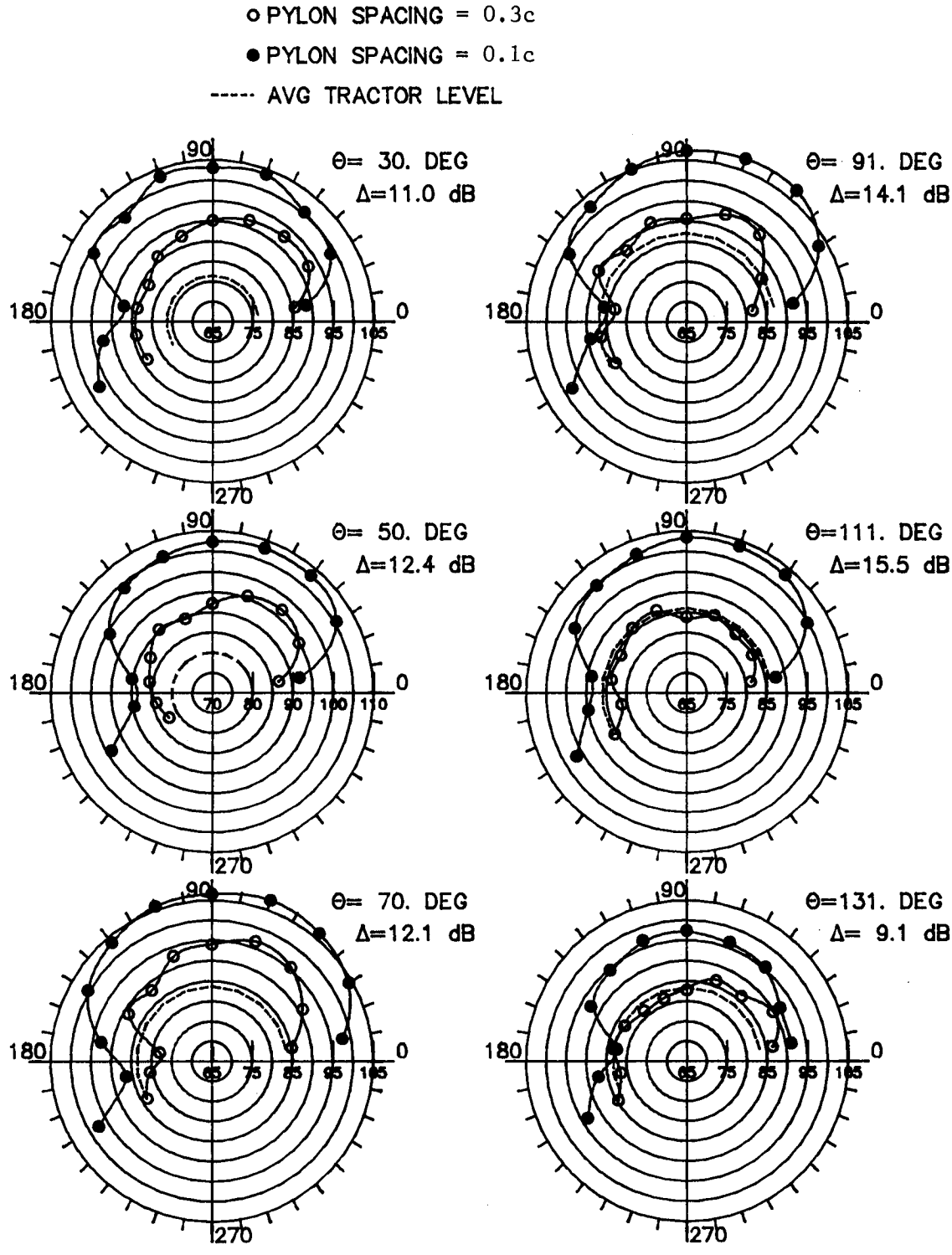

Figure 24. OASPL directivity comparisons for $0.1c$ and $0.3c$ spacing of radial pylon. $\beta_{.75} = 30.0°$; eight blades. 7200 rpm; $M_T = 0.456$; $(\mathrm{SHP}/d^2)/B = 1.0$ hp/ft^2.

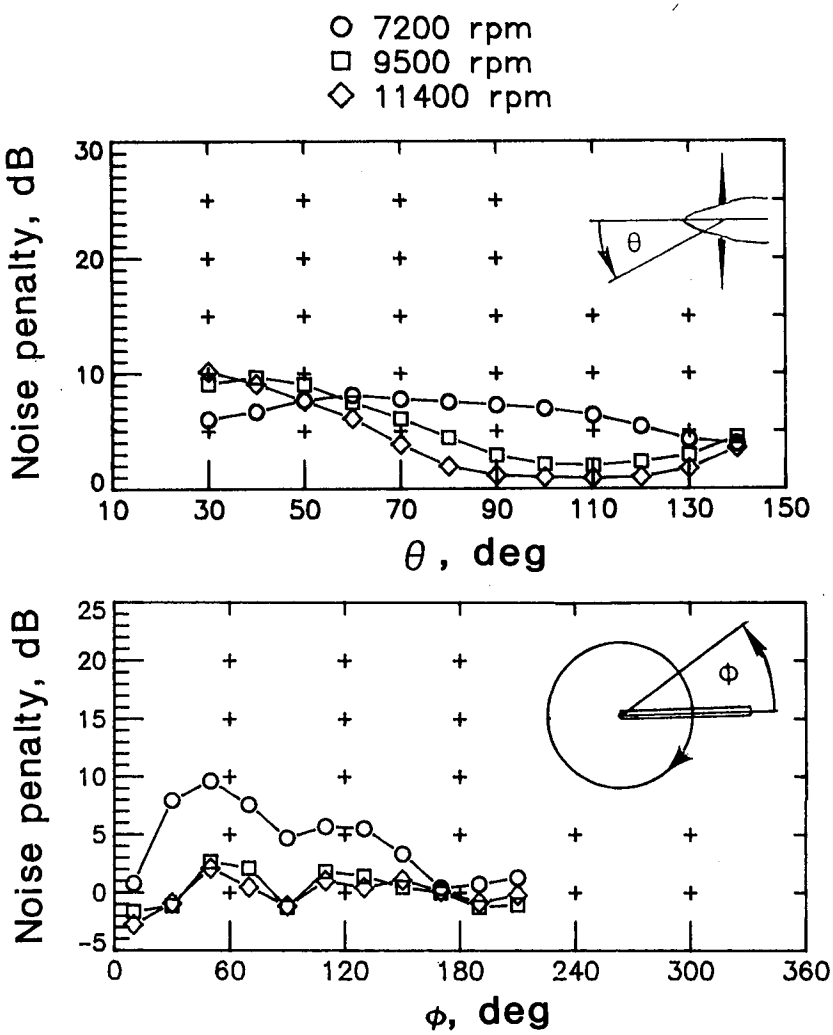

Figure 25. Variation of noise penalty with θ and ϕ for pylon spacing of $0.1c$ compared with pylon spacing of $0.3c$. $\beta_{.75} = 18.8°$; four blades.

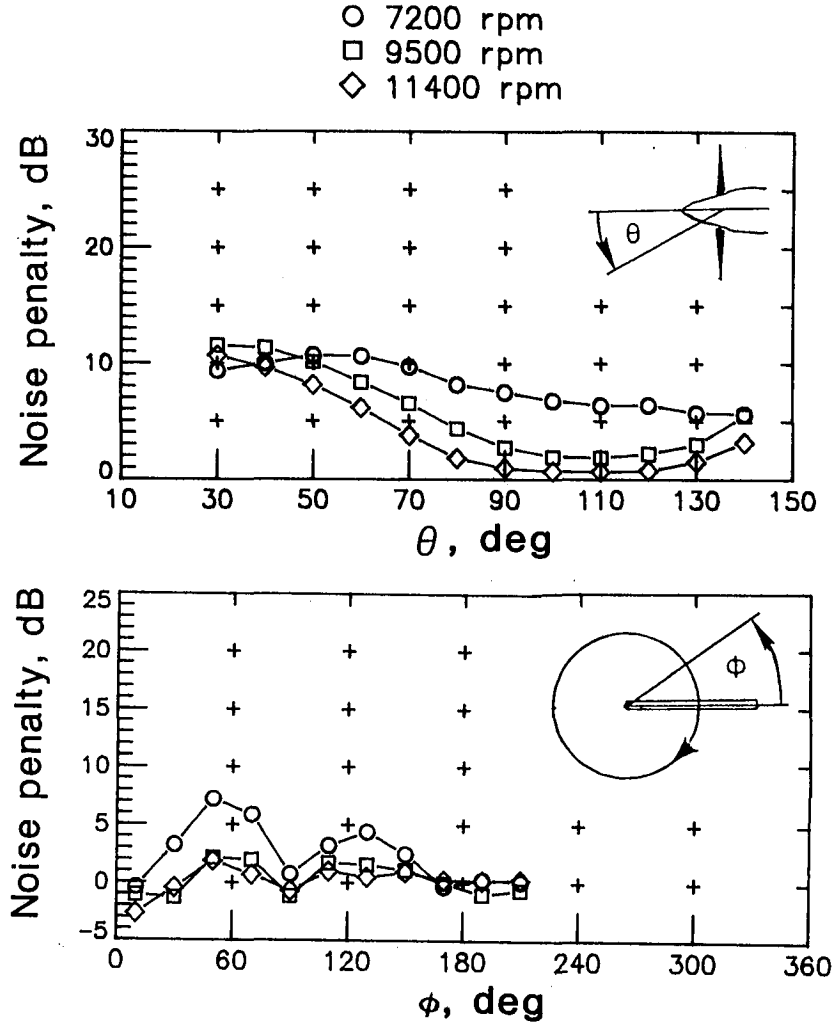

Figure 26. Variation of noise penalty with θ and ϕ for pylon spacing of $0.1c$ compared with pylon spacing of $0.3c$. $\beta_{.75} = 24.0°$; four blades.

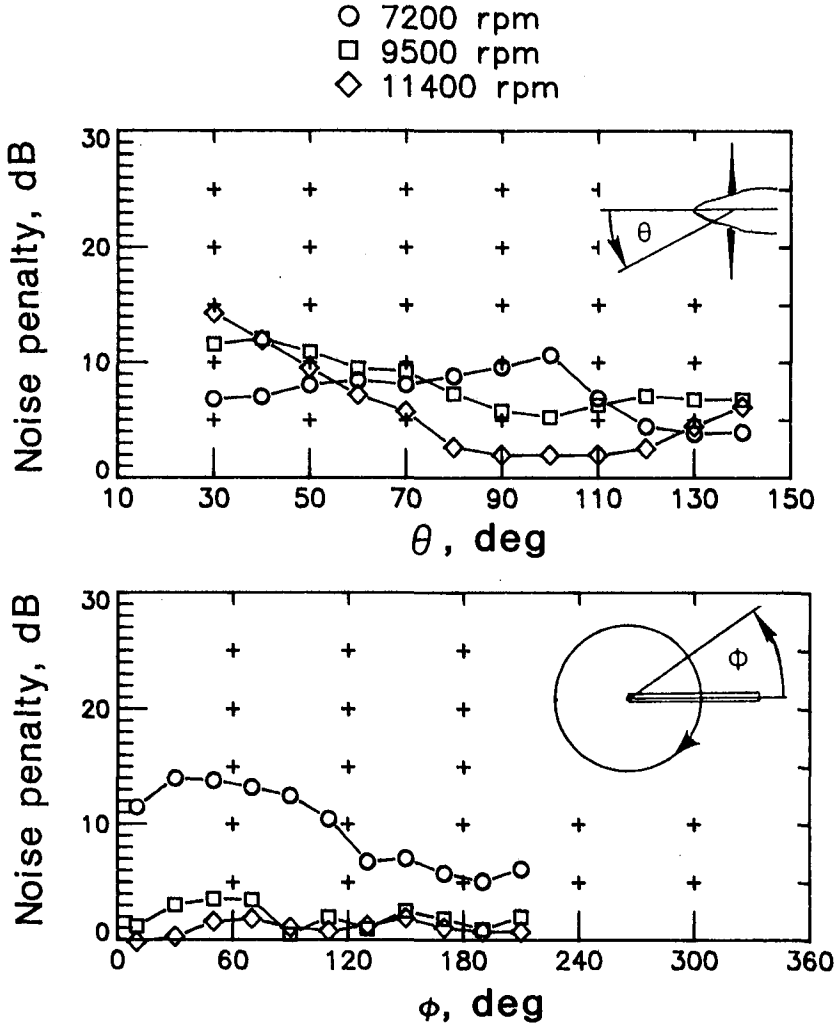

Figure 27. Variation of noise penalty with θ and ϕ for pylon spacing of $0.1c$ compared with pylon spacing of $0.3c$. $\beta_{.75} = 20.0°$; eight blades.

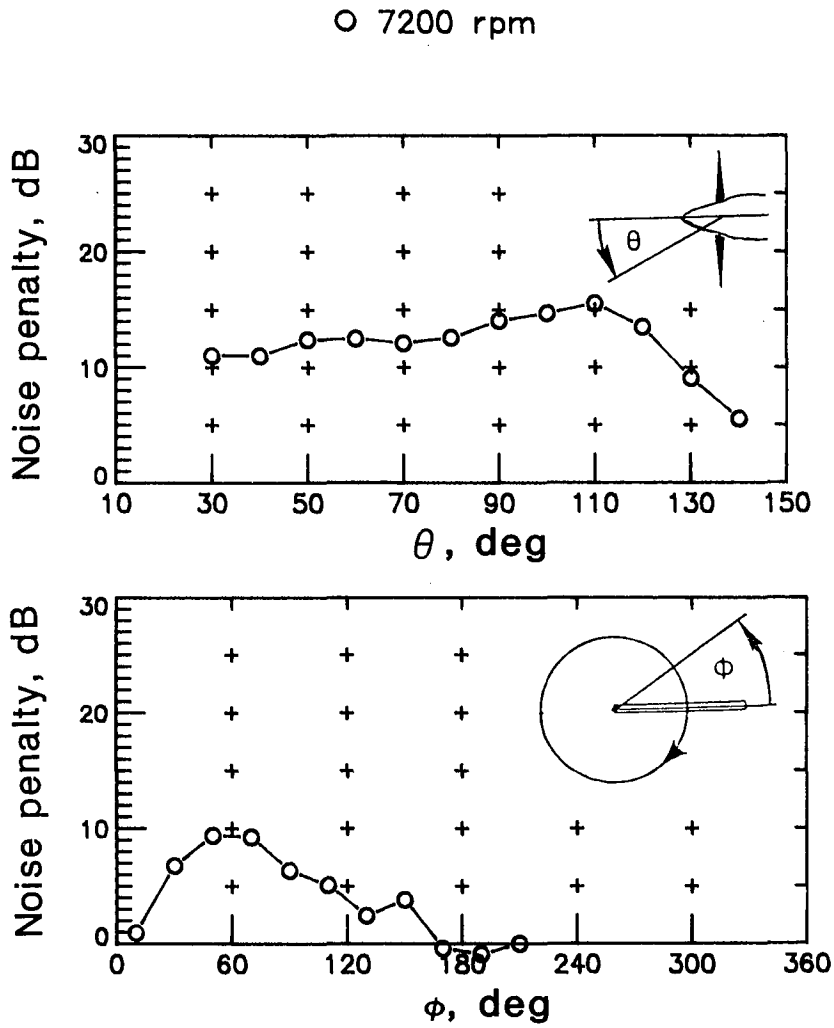

Figure 28. Variation of noise penalty with θ and ϕ for pylon spacing of $0.1c$ compared with pylon spacing of $0.3c$. $\beta_{.75} = 30.0°$; eight blades.

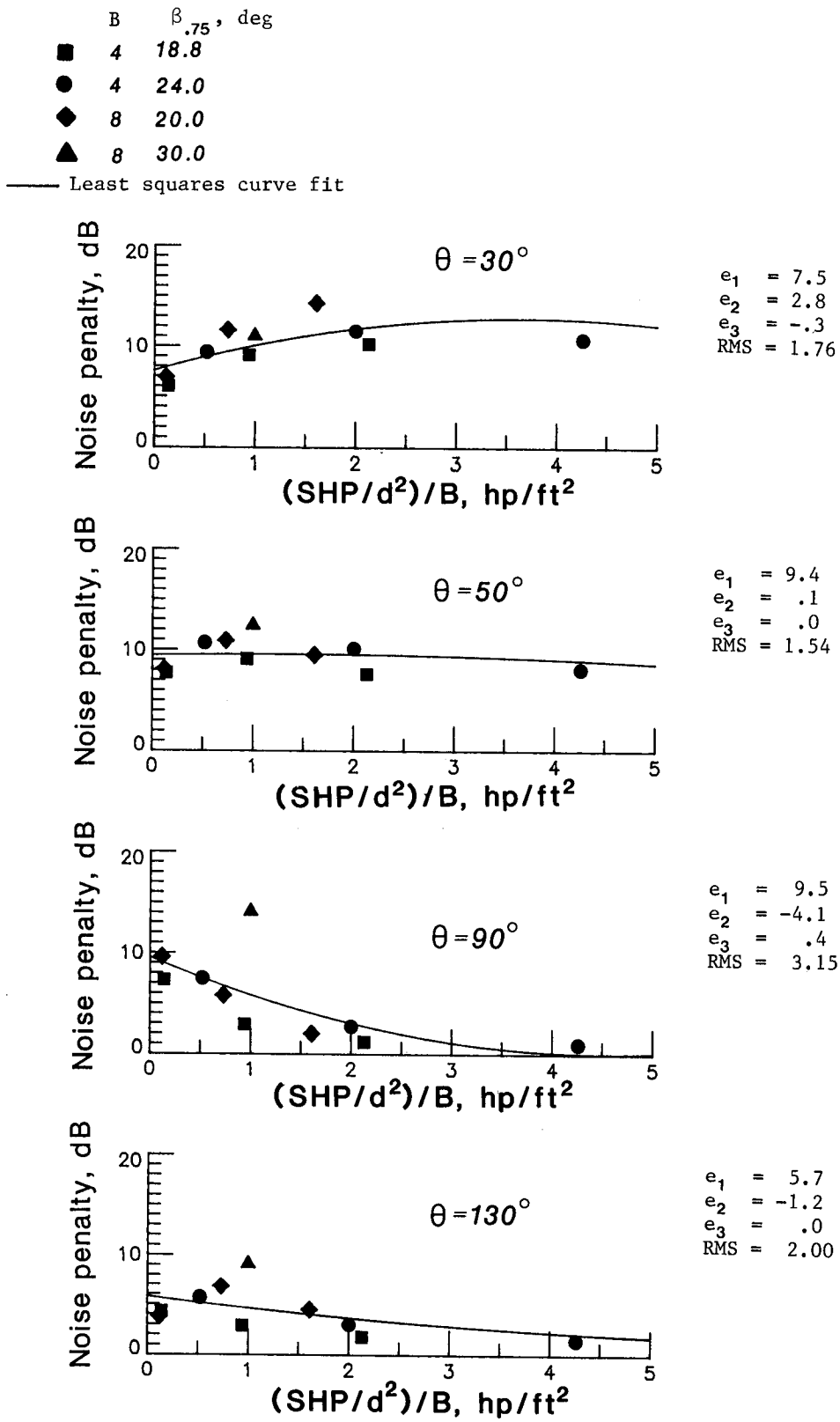

Figure 29. Trends in spacing noise penalty with $(\mathrm{SHP}/d^2)/B$ at selected values of θ.

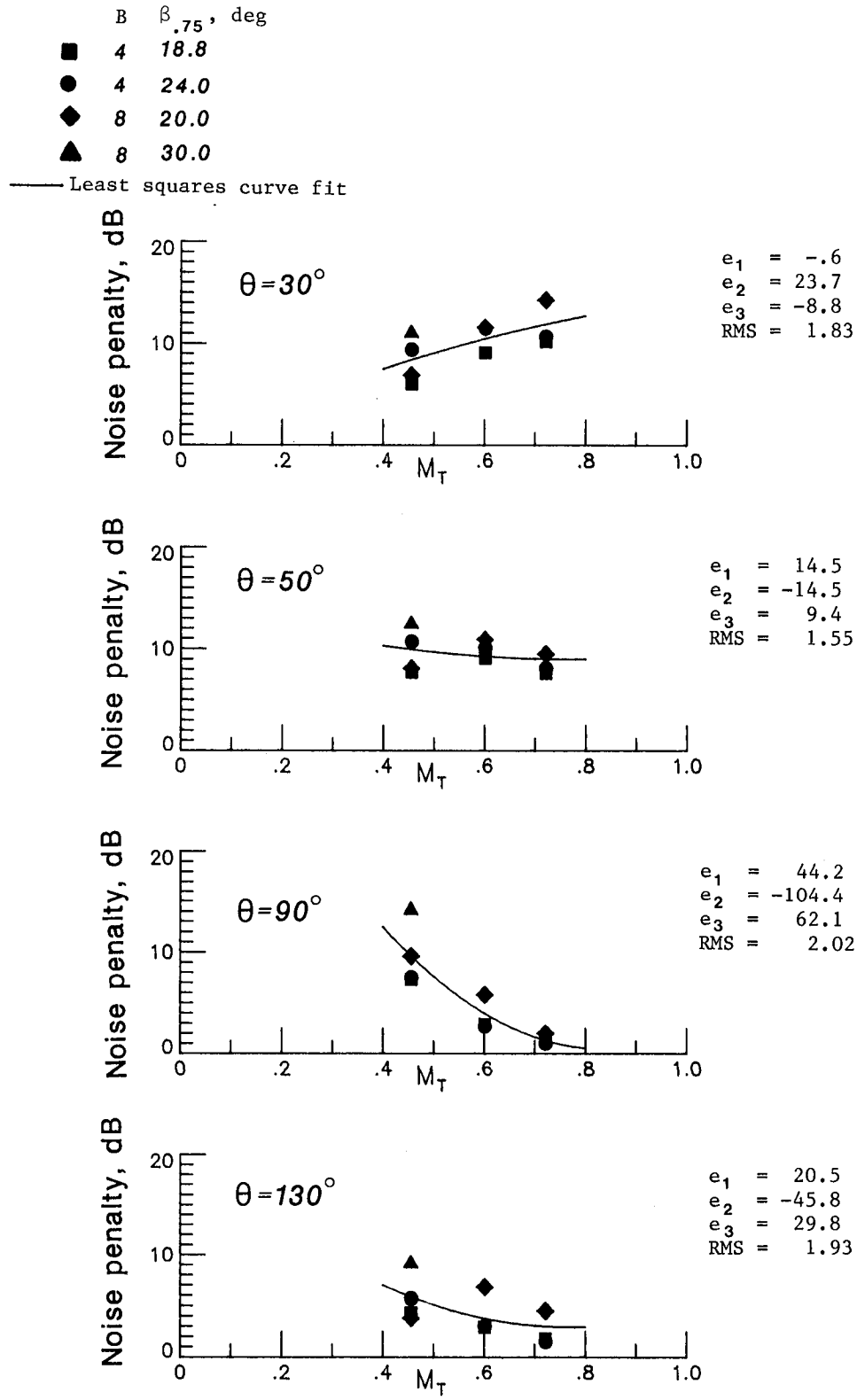

Figure 30. Trends in spacing noise penalty with M_T at selected values of θ.

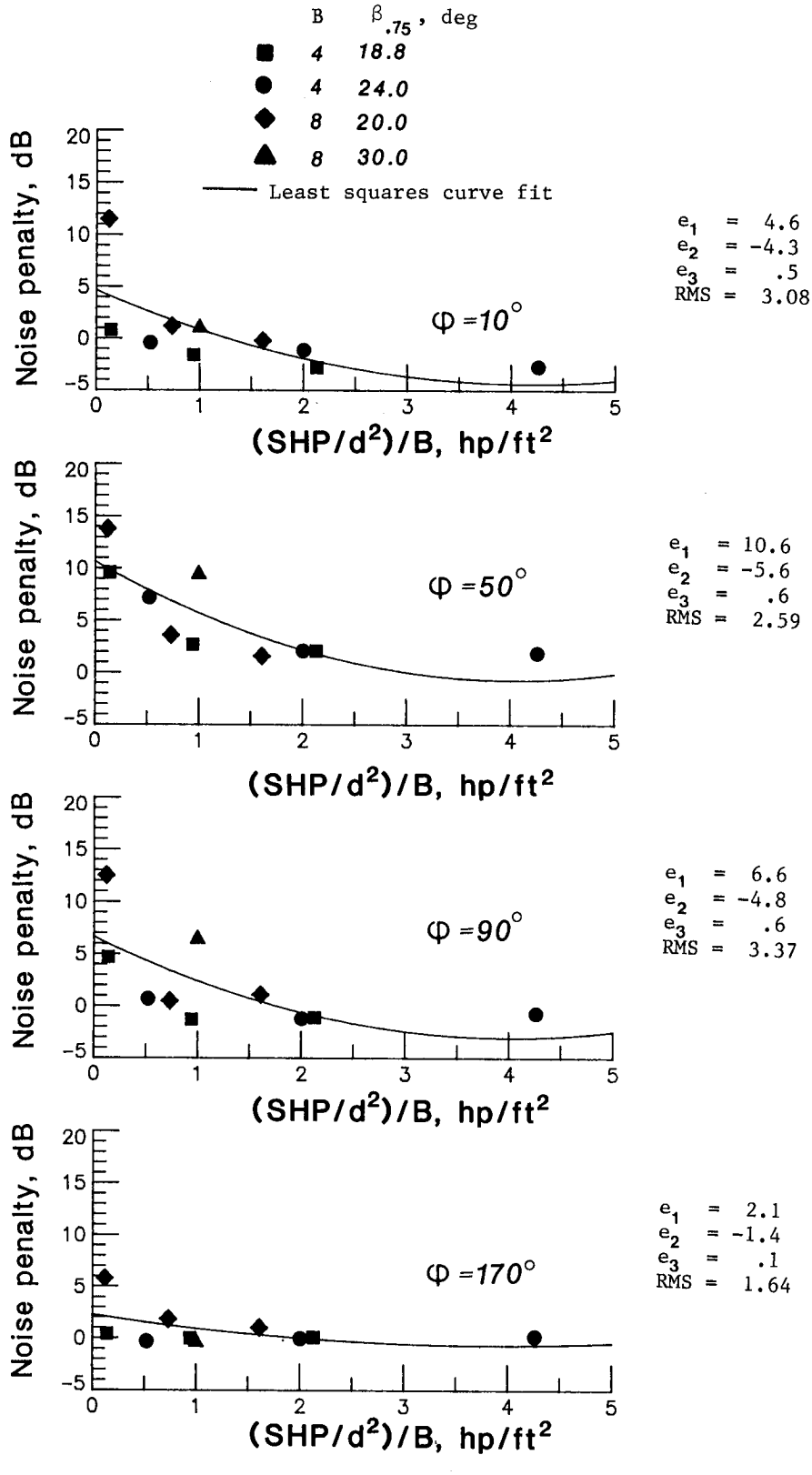

Figure 31. Trends in spacing noise penalty with $(\mathrm{SHP}/d^2)/B$ at selected values of ϕ.

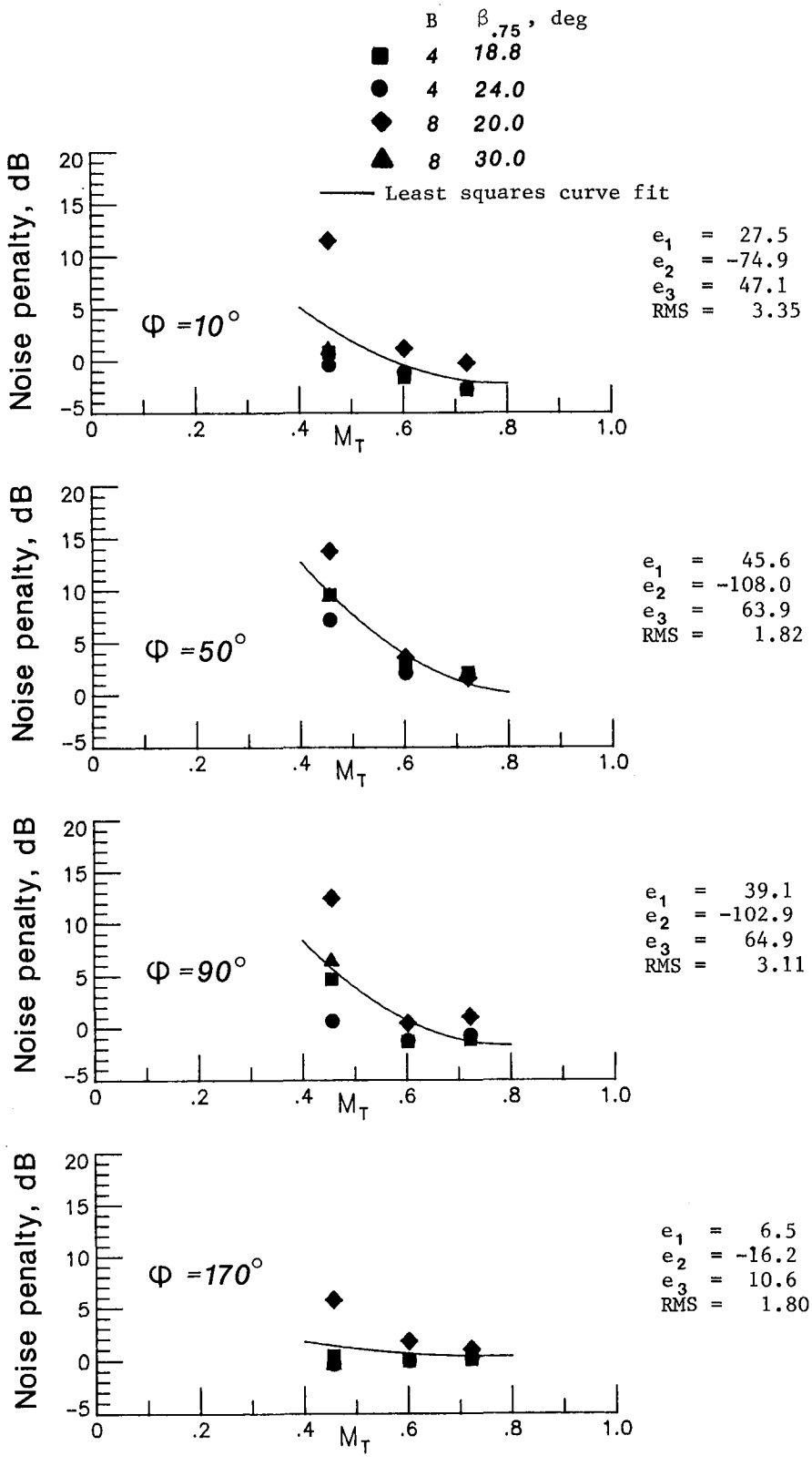

Figure 32. Trends in spacing noise penalty with M_T at selected values of ϕ.

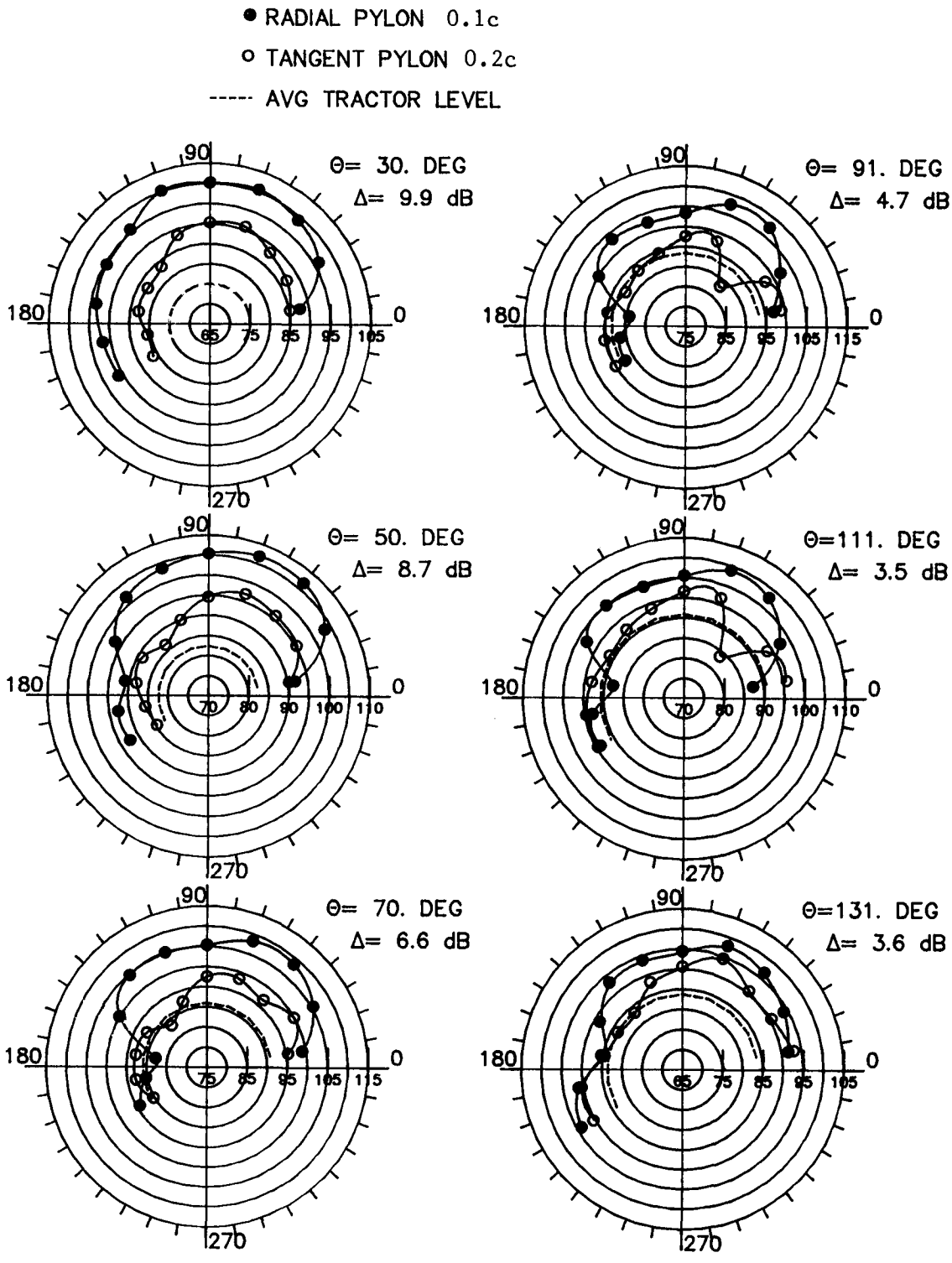

(a) 7200 rpm; $M_T = 0.456$; $(\mathrm{SHP}/d^2)/B = 0.52$ hp/ft^2.

Figure 33. OASPL directivity comparisons for radial ($0.1c$) and tangent ($0.2c$) pylons. $\beta_{.75} = 24.0°$; four blades. Plotted data are OASPL values in decibels. Circumferential angles ϕ are in degrees.

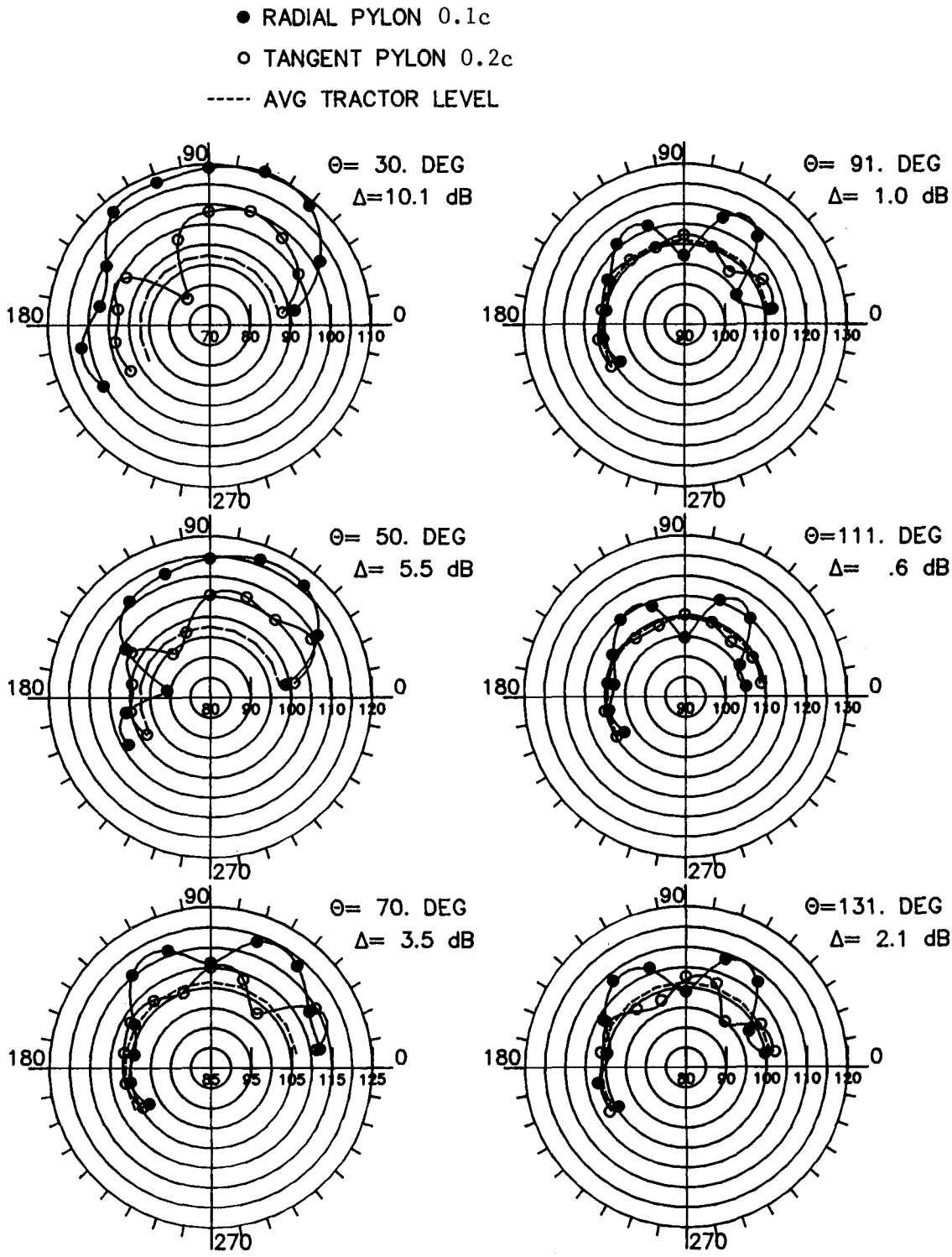

(b) 9500 rpm; $M_T = 0.601$; $(\mathrm{SHP}/d^2)/B = 2.0$ hp/ft^2.

Figure 33. Continued.

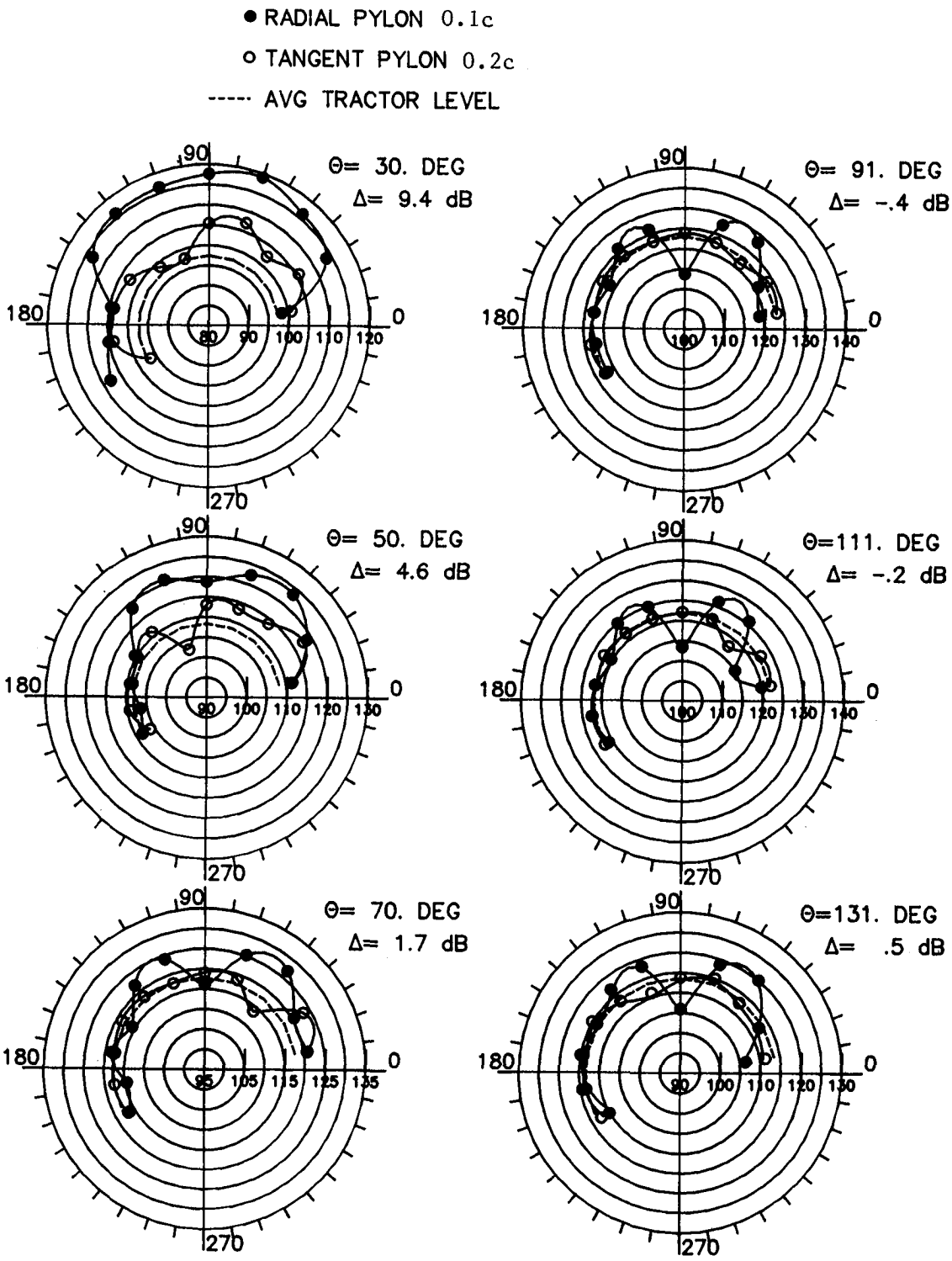

(c) 11 400 rpm; $M_T = 0.722$; $(\mathrm{SHP}/d^2)/B = 4.26$ hp/ft^2.

Figure 33. Concluded.

Standard Bibliographic Page

1. Report No.	2. Government Accession No.	3. Recipient's Catalog No.
NASA TP-2609		

4. Title and Subtitle	5. Report Date
Directivity and Trends of Noise Generated by a Propeller in a Wake	September 1986
	6. Performing Organization Code: 535-03-11-02
7. Author(s): P. J. W. Block and Garl L. Gentry, Jr.	8. Performing Organization Report No.: L-16131
9. Performing Organization Name and Address: NASA Langley Research Center, Hampton, VA 23665-5225	10. Work Unit No.
	11. Contract or Grant No.
12. Sponsoring Agency Name and Address: National Aeronautics and Space Administration, Washington, DC 20546-0001	13. Type of Report and Period Covered: Technical Paper
	14. Sponsoring Agency Code

15. Supplementary Notes

16. Abstract

An experimental study of the effects on far-field propeller noise of a pylon wake interaction was conducted with a scale model of a single-rotation propeller in a low-speed anechoic wind tunnel. A detailed mapping of the noise directivity was obtained at 10 test conditions covering a wide range of propeller power loadings at several subsonic tip speeds. Two types of noise penalties were investigated–"pusher" and "spacing." The pusher noise penalty is the difference in the average overall sound pressure level, OASPL, for pusher and tractor installations. (In a pusher installation, the propeller disk is downstream of a pylon or another aerodynamic surface.) The spacing noise penalty is the difference in the average OASPL for different distances between the pylon trailing edge and the propeller. The variations of these noise penalties with axial, or flyover, angle θ and circumferential angle ϕ are presented, and the trends in these noise penalties with tip Mach number and power loading are given for selected values of θ and ϕ. The circumferential directivity of the noise from a pusher installation showed that the additional noise due to the interaction of the pylon wake with the propeller had a broad peak over a wide range of circumferential angles approximately perpendicular to the pylon with a sharp minimum 90° to the pylon for the majority of cases tested. The variation of the pusher noise penalty with θ had a minimum occurring near the propeller plane and maximum values of as much as 20 dB occurring toward the propeller axes. The magnitude of the pusher noise penalty generally decreased as propeller tip Mach number or power loading was increased. However, the penalty did not decrease to zero in all directions.

17. Key Words (Suggested by Authors(s))	18. Distribution Statement
Aerodynamic noise Aircraft wake Propellers Propeller noise Acoustic measurement Low-speed wind tunnels	Unclassified—Unlimited Subject Category 71

19. Security Classif.(of this report)	20. Security Classif.(of this page)	21. No. of Pages	22. Price
Unclassified	Unclassified	62	A04

For sale by the National Technical Information Service, Springfield, Virginia 22161

NASA-Langley, 1986

NASA